Apolipoprotein L9 interacts with LC3/GABARAP and is a microtubule-associated protein with a widespread subcellular distribution

Arvind A. Thekkinghat[1]*, Kamlesh K. Yadav[1,2] and Pundi N. Rangarajan[1]*

[1]Department of Biochemistry, Indian Institute of Science, Bangalore, 560012, INDIA

[2]Present address: National Institute of Diabetes and Digestive and Kidney Diseases, National Institutes of Health, Bethesda, MD, 20892, USA

* Correspondence: arvinda@iisc.ernet.in (A.A.T); pnr@iisc.ac.in (P.N.R)

Keywords: Apolipoprotein L9**,** phosphatidylethanolamine, autophagy, microtubules, lysosomes, LC3/GABARAP

Abstract

Mouse Apolipoprotein L9 is a 34-kDa phosphatidylethanolamine (PE)-binding protein. The gene is present only in mouse and rat genomes; hence it is taxonomically restricted. To understand why, it is essential to uncover details about its functions in cellular processes. Here we show that ApoL9 interacts with the proteins of the LC3 and GABARAP subfamilies, which are key players in macroautophagy. In amino-acid starved cells it preferentially interacts with lipidated LC3B, likely by binding to its PE moiety. On treatment with autophagy inhibitors bafilomycin A1 and chloroquine, ApoL9 is found near swollen mitochondria and on lysosomes/LAMP1-positive compartments. However, ApoL9 itself does not seem to be degraded as a result of autophagy, suggesting that it is not an autophagy cargo receptor. Deletions in a putative transmembrane region between amino acids 110 and 145 abolish PE-binding. In addition, ApoL9 can redistribute to stress granules, can homooligomerize, and is a microtubule-associated protein. In short, its distribution in the cell is quite widespread, suggesting that it could have functions at the intersection of membrane binding and reorganization, autophagy, cellular stress and intracellular lipid transport.

Summary statement

This article is about how Apolipoprotein L9, a lipid-binding protein, has versatile properties and influences a variety of processes taking place inside an animal cell.

50 ## Introduction

51 Mouse ApoL9, encoded by two independent genes *Apol9a* and *Apol9b* on chromosome 15, has
52 previously been shown to have either antiviral or pro-viral effects during infection of cells by
53 different types of viruses (Kreit et al., 2014; Kreit et al., 2015; Arvind and Rangarajan, 2016).
54 Expression of ApoL proteins is also induced by interferons and TNF-α (Zhaorigetu et al., 2011,
55 Monajemi et al., 2002). Small quantities of ApoL9 secreted from macrophages during interferon
56 induction have been shown to promote epithelial cell proliferation in a paracrine fashion (Sun et al.,
57 2015). However, most of the protein is retained within the cell. In a previous study, we used B16F10
58 melanoma cells to look at the basic expression pattern of constructs expressing ApoL9, examined its
59 levels in various mouse tissues, and viewed it in the context of infection by Japanese Encephalitis
60 virus (Arvind and Rangarajan, 2016). We reported that ApoL9 is a phosphatidylethanolamine-binding
61 protein that, in normal conditions, has a general cytoplasmic distribution and can localize to
62 ubiquitin-positive bodies called ALIS (aggresome-like induced structures) and aggresomes. ApoL9 is
63 expressed at moderate to high levels in mouse liver and brain, suggesting some function of
64 relevance for the protein in these major tissues.

65 In order to understand the functions of ApoL9, it is essential to know more about its distribution in
66 the cell and the proteins it interacts with. In this study, our objective is to attempt to uncover as
67 many clues as possible to help place ApoL9 in the context of processes taking place in the cell. Since
68 phosphatidylethanolamine has a unique function as a modifier of autophagosome marker proteins
69 Atg8 and its orthologues (Kabeya 2004), we examined whether ApoL9 could influence autophagy.
70 We investigate how ApoL9 interacts with PE by screening deletion mutants of the protein for PE-
71 binding. We also investigate the fate of ApoL9 when cells are subjected to stress, by subjecting cells
72 to treatments that induce cell stress, and observe the distribution and levels of ApoL9 under these
73 conditions. We find that ApoL9 is a dynamic protein that localizes to various compartments in the
74 cell under different conditions.

75 ## Results

76 **1. ApoL9 interacts with the mammalian orthologues of Atg8**

77 We previously reported that ApoL9 localizes to ALIS-like structures, which also contain LC3 and
78 SQSTM1 (sequestosome 1/p62), proteins that have key roles in autophagic processes (Arvind and
79 Rangarajan, 2016). ApoL9 also binds PE, whose covalent modification of LC3 is a crucial event in the
80 initiation and progression of macroautophagy (henceforth referred to as autophagy). Several

81 proteins that regulate autophagy interact with LC3 and its homologues, which are central players in
82 autophagy (Wild et al., 2013). We investigated to check if ApoL9 could also interact with any of these
83 proteins. Mouse *Lc3a*, *Lc3b*, *Gabarap*, *Gabarapl1*, and *Gabarapl2* were expressed as Glutathione S-
84 transferase fusion proteins in *E.coli*, bound to glutathione-agarose, and examined for their ability to
85 interact with V5-tagged ApoL9 (ApoL9-V5) expressed in HEK293T cells. SDS-PAGE followed by
86 immunoblotting with anti-V5 antibody revealed that ApoL9 interacts with all the members of the
87 LC3 and GABARAP subfamilies, and that the interaction was strongest with GABARAP and
88 GABARAPL1 **(Fig. 1A).** To validate this interaction in vivo, we attempted to co-immunoprecipitate
89 GABARAP along with ApoL9. Using anti-V5 agarose, GABARAP could be immunoprecipitated along
90 with ApoL9-V5 from HEK293Tcells transfected with both *Apol9-V5* and *GFP-Gabarap* constructs **(Fig.**
91 **1B)**. GFP-LC3B could also be co-immunoprecipitated with ApoL9-V5 in a similar fashion, indicating
92 that ApoL9 interacts with both these proteins inside the cell.

93 Since the conversion of the cytosolic form of LC3 (LC3-I) to LC3-PE conjugate (LC3-II) occurs at the
94 onset of autophagy (Kabeya, 2000), we investigated if overexpression of ApoL9 had any influence on
95 levels of lipidated LC3 (LC3-II). HEK293T cells were transfected with either control plasmid or plasmid
96 expressing *Apol9-V5*, and to induce autophagy the cells were starved of amino acids by culturing in
97 Earle's Balanced Salt Solution (EBSS) for different time periods. Immunoblotting did not reveal any
98 significant difference in levels of LC3-II between the two conditions **(Fig. 1C)**, suggesting that ApoL9
99 expression does not alter levels of lipidated LC3, at least under conditions of amino acid starvation.

100 **2. ApoL9 localises to mitochondria and LAMP1-positive structures during treatment with**
101 **compounds that inhibit autophagy/induce mitochondrial damage**

102 When B16F10 melanoma cells stably expressing ApoL9-V5 ($B16F10^{L9}$) cells were treated with
103 bafilomycin A1, a V-ATPase inhibitor which inhibits the degradative capacity of lysosomes (Mauvezin
104 et al., 2015), the distribution of ApoL9 in the cell was significantly altered. Starting approximately 8-
105 10 h after treatment, three different patterns could be observed –localisation in the juxtanuclear
106 region, ring-like structures in the cytoplasm, and thread-like, highly curved/entangled structures in
107 the cytoplasm at later time points **(Fig. 2A)**. The juxtanuclear ApoL9 co-localized with structures
108 stained by an anti-LAMP1 antibody, indicating that they were lysosomes or other LAMP1-positive
109 structures **(Fig. 2B)**. The ring-like structures positive for ApoL9 increased in number with time, and
110 co-localized with the outer mitochondrial marker protein TSPO, indicating that they were swollen
111 mitochondria **(Fig. 2C)**. The curved, thread-like structures also increased in number with time, but
112 did not co-localize with any organelle marker we used **(Fig. 2B, C)** .These three patterns are not
113 mutually exclusive, but we often notice that cells in which juxtanuclear lysosomal localization

114 predominates contain fewer curved, thread-like structures and vice versa. Thus, the possibility these
115 two patterns are linked cannot be ruled out.

116 We also noticed ApoL9 localizing to ring-like mitochondria, starting approximately 8-10 h post
117 treatment with brefeldin A **(Fig. 2D)**, an ER stress inducer that inhibits protein transport from the ER
118 to the Golgi apparatus by inhibiting a guanine nucleotide exchange factor GBF1, causing a collapse of
119 the proteins into the ER (Fujiwara et al., 1988; Niu et al., 2005). ApoL9 was only found on some
120 mitochondria, but not all **(Fig. 2E)**, during treatment by either brefeldin A or bafilomycin A1, and this
121 number steadily increased with incubation time with these compounds. ER stress induced by
122 brefeldin A has previously been shown to damage mitochondria by depolarizing them, triggering
123 apoptosis by the classical pathway (Lee et al., 2013). Bafilomycin A1 has been demonstrated to be a
124 potassium ionophore that leads to impairment of mitochondrial functions by causing them to swell
125 and lose membrane potential (Teplova et al., 2007). These properties of the compounds, and the
126 considerable time period after which ApoL9 localises to mitochondria in B16F10^{L9} cells during
127 treatment with these compounds, are indications that the ApoL9-positive mitochondria might have
128 suffered damage to their integrity.

129 There are clear differences between ApoL9 localization during treatment with bafilomycin A1 and
130 brefeldin A. During treatment with brefeldin A, ApoL9 localizes only to TSPO-positive ring-like
131 structures which are swollen mitochondria. These are often seen clustered together, appearing to be
132 in contact **(Fig. 2D)**. No localization to lysosomes **(Fig. S1.A)** or to curved thread-like structures can
133 be seen. Also, the fluorescence signal from ApoL9 becomes weaker with time, unlike in the case of
134 bafilomycin A1 treatment.

135 In bafilomycin A1-treated cells, LC3B (as GFP-LC3B) accumulates in numerous punctate
136 autophagosomes due to the downstream block in autophagy. ApoL9 does not localize to these
137 structures, suggesting that it is not a part of the autophagosome per se, though transient
138 interactions with autophagosomes might occur **(Fig. 2F)**. Upon treatment with bafilomycin A1 and
139 brefeldin A, LC3B and GABARAP also appear in the vicinity of mitochondria along with ApoL9, which
140 might indicate that the autophagic machinery is recruited to the damaged mitochondria **(Fig.2G, H,**
141 **and S1.B)**. In some cases there appears to be only partial colocalization between ApoL9 and
142 TSPO/LC3B, suggesting that they might be part of more than one structure on or near the
143 mitochondria. But spatial restriction of LC3B/GABARAP localization to ApoL9-positive mitochondria
144 is very clearly evident. The presence of ApoL9 on LAMP-1-positive structures and swollen
145 mitochondria when autophagy is inhibited, and its co-localization with LC3B and GABARAP, suggests
146 a role in autophagy.

147 Another phenomenon observed in cells treated with bafilomycin A1 is the presence of a number of
148 the ApoL9-positive ring-like structures outside the boundaries of the cells that once contained them.
149 They could be seen well outside the boundary of the cells, exiting the membrane **(Fig. 2I)**, or in close
150 contact with the membrane (before exit), in various images **(Fig. S1.C,D)**. Mitochondria have
151 previously been described to be ejected from cells undergoing phenomena such as necroptosis and
152 serve as a source of DAMPs (damage-associated molecular patterns) (Maeda and Fadeel, 2014;
153 Krysko et al., 2011). This study is the first report of ApoL9-containing mitochondria in the
154 extracellular milieu, though it is not clear how much the mitochondria inside the cells and
155 mitochondria outside the cells differ in membrane integrity and protein composition. We didn't
156 observe this phenomenon in cells treated with brefeldin A.

157 **3. ApoL9 accumulates in the Triton X-100-insoluble fraction of lysates of cells treated with**
158 **bafilomycin A1, but does not seem to be a receptor for selective autophagy**

159 In western blots of cell lysates of B16F10^{L9} cells treated with bafilomycin A1, there is a gradual
160 decrease of ApoL9 in the Triton X-100 soluble fraction and a corresponding increase in the insoluble
161 fraction **(Fig. 3A)**, which correlates with the gradual accumulation of ring-like, curved or thread-like
162 entangled structures in the cytoplasm over the same time period.

163 ApoL9 protein levels in B16F10^{L9} cells were seen to decrease with time during treatment with
164 brefeldin A **(Fig. 3B)**. A similar decrease was seen in endogenous ApoL9 in H6 hepatoma cells **(Fig.**
165 **3C)**. qPCR from H6 hepatoma cells treated with brefeldin A reveals that there is no decrease in
166 ApoL9 mRNA levels during this treatment, indicating that reduced protein levels are not due to a
167 decrease in the transcription of the *Apol9* genes **(Fig. 3D)**. Further, amino acid starvation of
168 B16F10^{L9} cells (treatment with EBSS) led to a decrease in ApoL9 levels with time **(Fig. 3E)**. To
169 determine if this decrease was due to autophagy, or if ApoL9 was being degraded as a result of the
170 autophagic process, the cells were treated with the autophagy inhibitor bafilomycin A1 in
171 combination with starvation. Bafilomycin A1 was not able to prevent the decrease in ApoL9 protein
172 levels during amino acid starvation **(Fig. 3F)**. It is important to note that bafilomycin A1 does not
173 exert its aforementioned effects on the ApoL9 localization pattern during the timescale of the
174 experiment involving starvation with EBSS (6 hours). A similar time-dependent decrease in ApoL9
175 levels was also noticed when B16F10^{L9} cells were treated with cycloheximide, an inhibitor of protein
176 synthesis **(Fig. 3G)**. Therefore, it seems that the decrease in ApoL9 levels during amino acid
177 starvation or treatment with brefeldin A is reflective of normal turnover of ApoL9 in the cell, likely
178 due to decreased protein synthesis in the cell during starvation and ER stress, rather than the result
179 of autophagic degradation. We have previously shown that ApoL9 is primarily degraded by

180 proteasomes, as evidenced by an increase in ApoL9 levels in MG132-treated cells (Arvind and
181 Rangarajan, 2016).

182 **4. On treatment with chloroquine, ApoL9 shows a clustered pattern of staining, localises to**
183 **LAMP1-positive structures and interacts with LC3-II**

184 Like bafilomycin A1, chloroquine (CQ) is also an inhibitor of autophagy. It is a lysosomotropic agent
185 that was thought to accumulate inside lysosomes and reduce their acidity, but it has recently been
186 determined that chloroquine actually inhibits autophagy by preventing autophagosome-lysosome
187 fusion, in addition to having disorganizing effects on the Golgi and endo-lysosomal systems (Mauthe
188 et al., 2018). Treatment of B16F10^{L9} cells with chloroquine resulted in a clustered pattern of ApoL9 in
189 the cytoplasm. Coupling amino acid starvation with CQ treatment (to induce autophagy and
190 simultaneously prevent autophagic degradation) hastened the formation of these clusters and
191 produced a more pronounced pattern for a given time period as compared with treatment with CQ
192 alone **(Fig. 4A)**. The ApoL9 in these clusters/vesicles partially colocalized with LAMP1, suggesting
193 that it was interacting with lysosomes or other LAMP1-positive vesicles that are known to be derived
194 from lysosomes **(Fig. 4B)**. When a cell line stably expressing V5-tagged LC3B (B16F10^{LC3B}) was treated
195 with CQ and EBSS, a similar pattern is observed with LC3B displaying partial but slightly higher
196 degree of co-localization with LAMP1-positive structures, indicating that these are autophagic
197 vesicles, since LC3B is primarily a marker of autophagosomes **(Fig. 4C)**. This clearly indicates that
198 ApoL9 is involved in autophagy triggered by amino acid starvation. Treatment with CQ alone does
199 not lead to a build-up of ApoL9 levels in the cell **(Fig. 4D)**, nor does CQ prevent the decrease in
200 ApoL9 levels caused by amino acid starvation **(Fig. 4E)**. Thus it is unlikely that ApoL9 functions as a
201 cargo receptor that is degraded during selective autophagy.

202 Since ApoL9 and LC3B display similar patterns of distribution in amino acid-starved, CQ-treated cells,
203 we decided to examine their interaction during this treatment. HEK293T cells transfected with
204 *Apol9-V5* were subjected to amino acid starvation coupled with chloroquine treatment for different
205 time points to prevent autophagic degradation, thereby causing accumulation of LC3-II. When the
206 cell lysates were incubated with anti-V5 agarose to immunoprecipitate ApoL9-V5, LC3B was co-
207 immunoprecipitated along with ApoL9. Notably, only the LC3-II form was co-immunoprecipitated
208 **(Fig. 4F)**, indicating that ApoL9 has a strong affinity for LC3-II. To corroborate this finding,
209 recombinant MBP (maltose binding protein) and MBP-ApoL9 from *E.coli*, bound to amylose resin,
210 were incubated with untreated or chloroquine-EBSS-treated HEK293T lysates. Only LC3-II was pulled
211 down by MBP-ApoL9, confirming that ApoL9 interacts preferentially with that form of LC3 **(Fig. 4G)**.
212 This is likely to be a direct result of ApoL9 associating with the PE moiety of LC3-II, since there is

213 otherwise no discernible difference between the two LC3 forms. It is also a clear indication that
214 ApoL9 inside the cell interacts with the lipidated form of LC3 during starvation-induced autophagy,
215 thereby having the potential to influence the process. It must be remembered, from Fig.1A, that
216 ApoL9 has a strong affinity for GABARAP and GABARAPL1 even when these proteins are not in their
217 lipidated form.

218 **5a. Mutation of a potential LIR motif $_{67}$FPRL$_{70}$ weakens association of ApoL9 with GABARAP**

219 We have demonstrated that ApoL9 can not only interact with the lipidated form of LC3, but also with
220 nonlipidated LC3 homologues (Fig. 1A).To determine if ApoL9 contains an LIR (LC3-interacting
221 region) motif that is usually required for interaction with LC3/GABARAP family members (Birgisdottir
222 et al., 2013) and has the consensus sequence (W/F/Y)-X-X-(L/I/V), where 'X' is any amino acid, we
223 scanned the ApoL9 protein sequence for potential LIRs. Five potential LIRs were identified in the 310
224 amino acid sequence **(Fig. 5A)**. By site-directed mutagenesis, the codons encoding the 1st and 4th
225 (aromatic and hydrophobic) residues of these sequences were mutated to alanines in the ApoL9-V5
226 construct, generating LIR mutants M1-M5. These mutant proteins were expressed in HEK293T cells
227 and tested for binding to GST-GABARAP. LIR mutants M1, M2, M4, and M5 did not alter binding with
228 GABARAP either when mutated singly **(Fig. 5B)** or when all the four were simultaneously mutated
229 (data not shown). LIR M3, the sequence FPRL (67-70), when mutated to APRA resulted in severely
230 reduced expression of the *ApoL9-V5* construct in cells. When lysate quantities were normalized so as
231 to take equivalent quantities of wild type and mutant protein for the GABARAP pull-down assay, it
232 was seen that mutating this sequence reduced binding to GABARAP by about 50% (average of 3
233 experiments) **(Fig. 5C)**, indicating that the sequence FPRL (67-70) might function as an LIR in ApoL9.

234 **5b. ApoL9 molecules associate with each other**

235 We had reported earlier that the subcellular distribution pattern and morphology of ApoL9-GFP
236 fusions differed greatly from that of ApoL9 with smaller epitope tags, probably due to the larger size
237 of GFP (Arvind and Rangarajan, 2016). It was serendipitously observed that electroporation of *Apol9-*
238 *GFP* into B16F10^{L9} cells caused the ApoL9-V5 to redistribute in the typical pattern of ApoL9-GFP **(Fig.**
239 **5D)**, leading us to investigate if both forms of ApoL9 were associating with each other.

240 When MBP and MBP-ApoL9 bound to amylose resin were incubated with lysate of 293T cells
241 expressing ApoL9-V5, it was determined that ApoL9-V5 associated with MBP-ApoL9 but not with
242 MBP alone **(Fig. 5E)**. Further, immunoprecipitation of ApoL9 from lysates of cells transfected with
243 two forms of ApoL9 (*ApoL9-V5* and *ApoL9-3XFLAG*) demonstrated that ApoL9-3XFLAG could be
244 pulled down by ApoL9-V5, indicating that one form of ApoL9 could associate with the other **(Fig. 5F)**.

245 The ApoL proteins are BH3-only proteins, as they contain a putative BH3 domain that is
246 characteristic of the Bcl-2 family of proteins (Kreit et al., 2015). Since BH3 domains are known to be
247 involved in homo- and hetero-oligomerization between proteins containing them (Kale et al., 2018),
248 we tested whether deleting the core region of the BH3 domain of ApoL9 (amino acids 81-89) would
249 affect association between ApoL9 molecules. The results indicated that MBP-ApoL9-ΔBH3 was
250 severely impaired in its ability to interact with ApoL9-V5, when compared with wild type MBP-
251 ApoL9. **(Fig.5G)**. This indicated that the BH3 domain is involved in oligomerization of ApoL9
252 molecules. However, more pull-down experiments (*next section*) reveal that mutations in some
253 other regions also abolish the ability to associate with wild type ApoL9-V5, indicating that the
254 necessary for association/oligomerization might be spread over a wider region of the protein
255 sequence.

256 **6. Identification of the PE-binding region of ApoL9**

257 ***6a. Deletion of amino acids in a putative transmembrane region of ApoL9 abolishes binding to PE***

258 To identify the region of ApoL9 responsible for interaction with PE, we generated a series of mutants
259 carrying deletions in the ApoL9a protein sequence **(Fig. S2.A)**. All deletions were made in the MBP-
260 ApoL9 construct cloned in the vector pMAL-c2X. Various criteria were used for making the deletions
261 **(S2.B)**. The deletion constructs were expressed as MBP-fusion proteins in *E. coli*, which were purified
262 by amylose affinity chromatography **(Fig. S2.C)**. They were then used in protein-lipid overlay assays
263 to examine their ability to bind PE on nitrocellulose membrane, with wild type MBP-ApoL9 serving as
264 a positive control. The results indicated that both the deletions encompassing a putative
265 transmembrane region of the protein (Δ111-123, and Δ124-144; 'DAS' prediction server;
266 https://tmdas.bioinfo.se/DAS/index.html) abolished binding to PE **(Fig. 6A)**. Results obtained from
267 the two mutants carrying deletions in the BH3 domain and the C-terminal 30 amino acids were
268 inconclusive due to low levels of expression of the recombinant proteins, high levels of impurities
269 during purification and problems with reproducibility.

270 ***6b. Non-PE-binding mutants of ApoL9 differ in some of the properties exhibited by wild type ApoL9***

271 We subjected B16F10 cells expressing either ApoL9-V5-Δ111-123 or ApoL9-V5-Δ124-144 to various
272 treatments to see which of the properties displayed by wild type ApoL9 were abolished by deletions
273 in the transmembrane region involved in binding PE. We had reported previously that lipofection of
274 any plasmid into B16F10^{L9} cells caused rapid and dramatic aggregation of ApoL9 due to its
275 propensity to interact with dioleoylphosphatidylethanolamine (DOPE) in the transfection reagent
276 (Arvind and Rangarajan, 2016). So, firstly, lipofection of an empty (insert-less) plasmid into cells

277 stably expressing these mutants (B16F10$^{L9\ \Delta 111\text{-}123}$ or B16F10$^{L9\ \Delta 124\text{-}144}$) did not result in aggregation of
278 ApoL9, confirming that these mutants were unable to interact with the DOPE in Lipofectamine 2000
279 **(Fig. 6B)**. Secondly, the alterations of ApoL9 distribution in the cells when treated with bafilomycin
280 A1 and brefeldin A, notably the mitochondrial localization of ApoL9 and curved, thread-like
281 structures, were not seen in the mutants **(Fig. 6C, D)**. Interestingly, localization to juxtanuclear
282 lysosomes was still observed in bafilomycin A1 treated cells **(Fig. 6E)**. Further, the clustered pattern
283 of ApoL9 is not seen when treated with chloroquine-EBSS for shorter time periods, but localization
284 to lysosomes persisted on long-term treatment with chloroquine **(Fig. S3.A)**, suggesting that lipid-
285 binding is not linked to lysosomal localization per se, but is still involved in starvation-induced
286 changes in ApoL9 distribution. An interesting observation was that ApoL9-V5-Δ124-144 formed
287 aggresomes on MG132 treatment but ApoL9-V5-Δ111-123 did not (compare **Fig. 6C and 6D)**. This
288 was also reflected in the observation that protein levels of ApoL9-V5-Δ111-123 remained more or
289 less unchanged over time on treatment with brefeldin A or cycloheximide, indicating poor turnover,
290 while those of ApoL9-V5-Δ124-144 decreased gradually with time **(Fig. S3.B,C)**, suggesting that the
291 region between amino acids 111 and 123 contains residues critical for facilitating proteasomal
292 degradation of ApoL9. Also, interaction with GABARAP remained undisturbed in both the mutants
293 **(Fig. S3.D)**, indicating that the transmembrane region had no role in mediating that interaction. On
294 the other hand, both mutant proteins lost the ability to associate with wild type ApoL9 **(Fig. S3.E)**,
295 indicating that the intactness of the region is a requisite for oligomerization to happen. A minor note
296 to make is that ApoL9Δ111-123 displays anomalous mobility in SDS-PAGE and migrates slightly
297 slower than wild type ApoL9 despite having a lower molecular mass.

298 **7. ApoL9 is a microtubule-associated protein**

299 We know that lipofection of an empty (insert-less) plasmid into B16F10^{L9} cells causes ApoL9-V5 to
300 aggregate in the cytoplasm (Arvind and Rangarajan, 2016; and Fig. 6B). But lipofection of an ApoL9-
301 V5-expressing plasmid into B16F10 cells presents a markedly different picture. In addition to a few
302 aggregates, ApoL9 is seen in several long, thin, fibre-like structures **(Fig. 7A)**. Further,
303 electroporation of ApoL9-V5 into cell lines such as HepG2 and HEK293T (which express high
304 quantities of protein) also resulted in such structures becoming visible **(Fig. 7B)**, ruling out that these
305 structures were another artefact of lipofection of ApoL9. Instead, we think that they are probably
306 formed as a result of high levels of ApoL9 protein expression, since lipofection is a remarkably
307 efficient transfection method that facilitates the expression of very high levels of protein per cell.

308 Since these structures resembled microtubules, we lipofected ApoL9-V5 into B16F10 cells and
309 treated the cells with either nocodazole or paclitaxel (Taxol), a microtubule depolymerizing agent

310 and a microtubule-stabilizing agent respectively. All fibre-like structures disappeared in ApoL9-
311 lipofected cells after a three-hour nocodazole treatment, while their abundance increased (including
312 in the cell periphery) on paclitaxel treatment **(Fig. 7C)**, indicating that ApoL9 localizes to
313 microtubules. Further, treatment of the B16F10^{L9} cell line with paclitaxel led to ApoL9-V5 becoming
314 visible on microtubules, which had become stabilized due to the effect of the drug **(Fig. 7D)**. Another
315 observation was that treatment of B16F10^{L9} cells with nocodazole greatly increased the number of
316 ALIS-like structures in the cytoplasm **(Fig. 7D)**, suggesting that the dynamics of ALIS in the cell are
317 regulated by microtubules and that attachment to microtubules might be involved in trafficking of
318 ApoL9 within the cell. Microtubule association was further confirmed by co-localization of ApoL9
319 with β-tubulin in paclitaxel-treated cells **(Fig. 7E)**. Also, GFP-tagged α-tubulin could be co-
320 immunoprecipitated with ApoL9-V5 from HEK293T cells transfected with both these proteins **(Fig.
321 7F)**, confirming that ApoL9 is a microtubule-associated protein (MAP). Both transmembrane deletion
322 mutants of ApoL9 failed to associate with microtubules, as evident from their immunofluorescence
323 pattern after treatment with paclitaxel, displaying no co-localization with tubulin **(Fig. S4.A)**. We
324 have sometimes seen the presence of β-tubulin in the curved, thread-like structures formed during
325 bafilomycin A1 treatment **(Fig. 7G)**. This observation has been sporadic and is not readily evident in
326 the majority of cells. But it probably suggests that microtubules are associated with these structures
327 at a certain point in the process of their formation, and might later dissociate from them. It is
328 pertinent to note that LC3B and its orthologues are also microtubule-associated proteins. It has been
329 shown previously that the first 22 amino acids of GABARAP have basic residues clustered on one side
330 of a helix that serves as a tubulin-binding motif (Wang and Olsen, 2000). ApoL9 being a protein that
331 mostly comprises helices in its secondary structure, we examined it for helices enriched in basic
332 residues. The region between amino acids 54 and 70, when visualized as a helical wheel, is part of a
333 helix with at least four basic residues (lysines) clustered on one side **(Fig. 7H)**. These lysines are also
334 conserved in the rat orthologue of ApoL9a **(Fig. S4.B)**. Further investigations will be needed to reveal
335 if this region indeed binds tubulin and, if yes, to elucidate structural details of the interaction.

336 **10. ApoL9 redistributes to stress granules under certain conditions of stress**

337 When B16F10^{L9} cells were subjected to heat stress by incubating them at 43˚C for 30 minutes,
338 ApoL9-V5 was seen to redistribute into a large number of granules in the cytoplasm. It was obvious
339 that these granules might be different from ALIS, due to their irregular size and shape, and higher
340 number. In addition to heat stress, we found that other conditions such as oxidative stress induced
341 by sodium arsenite or DTT (but not H_2O_2), and ER stress induced by thapsigargin, also caused the
342 redistribution of ApoL9 to such granules **(Fig. 8A)**. The identity of the granules was confirmed by co-

343 localization of ApoL9 with the well-known stress granule markers eIF3η (eukaryotic initiation factor
344 3η) and TIA-1 (T-cell intracytoplasmic antigen 1) **(Fig. 8A, Fig. S4.C)**. To confirm that ALIS and stress
345 granules were indeed different, we looked at the localization of SQSTM1 after thapsigargin
346 treatment. Double immunofluorescence showed that SQSTM1 localised to other granules but wasn't
347 present with ApoL9 in stress granules, confirming that these granules are not ALIS but bona fide
348 stress granules **(Fig. 8C)**. Curiously, these two granule types were in close apposition in many
349 locations in the cytoplasm, which could point towards a potential for interaction between their
350 components.

351 Neither of the transmembrane deletion mutants of ApoL9 ($ApoL9^{\Delta 111-123}$ or $ApoL9^{\Delta 124-144}$)
352 redistributed to these granules on subjecting to stress treatments, as evidenced by complete lack of
353 co-localization with eIF3η **(Fig. S.4D)**.

354

355 Discussion

356 Since ApoL9 is a phosphatidylethanolamine-binding protein, we hypothesised that this property is
357 likely to be the biggest determinant of the intracellular functions of the protein. Among the various
358 functions of PE in the cell, its role in autophagy stands out prominently. In this study, we have
359 carried out investigations primarily from this aspect. Each result obtained is discussed in detail in the
360 following paragraphs.

361 ***The possible implications of the ApoL9-LC3/GABARAP interaction***

362 One of the important results in this study is the demonstration of a direct interaction between the
363 lipidated form of LC3 and ApoL9 during starvation-induced autophagy. However, we do not observe
364 ApoL9 concentrated on the numerous punctate autophagosomes that appear in the cell during this
365 process, indicating that it is not an inherent part of the autophagosome. It is likely that ApoL9
366 transiently interacts with the expanding phagophore/maturing autophagosome. Further, ApoL9 also
367 interacts with the non-lipidated forms of LC3 and its homologues, with highest affinity for GABARAP
368 and GABARAPL1. Though we couldn't identify an LIR that completely abolished interaction with
369 GABARAP, it is worth noting that the key residues of the LIR motif candidate $_{67}FPRL_{70}$, mutation of
370 which reduced binding to GABARAP by >50%, are also conserved in rat ApoL9a. Though the
371 contributions of some other phospholipids (like the various phosphoinosides) in autophagy,
372 membrane remodelling, and mTOR regulation are well catalogued (Dall'Armi et al., 2013), the role of
373 PE in these processes is rather unclear. Shatz et al. state that, in addition to being conjugated with

374 LC3, PE might directly affect lipid bilayer properties of the autophagosome and isolation membrane
375 because it is a cone-shaped lipid and could influence curvature at the leading edge of the forming
376 autophagosome (Shatz et al., 2016). Nath et al. reported a direct correlation between the efficiency
377 of LC3 lipidation and the extent of curvature in lipid bilayers (Nath et al., 2014). Shatz et al. also
378 speculate that proteins with an LIR motif could facilitate docking of phagophore membrane
379 precursors by binding to LC3 on the formed phagophore or the incoming membrane during
380 phagophore formation. In this context, ApoL9 is unique in that it is capable of interacting with non-
381 lipidated LC3/GABARAP, lipidated LC3/GABARAP, with PE alone, as well as with other ApoL9
382 molecules, allowing a multidimensional range of possibilities as to how it might influence events at
383 the membrane during autophagosome formation. It would also be worth investigating the effect of
384 ApoL9 itself on membrane curvature, since it is associated with highly curved structures during
385 treatment with bafilomycin A1. Hsu and Shi state in their review of mitochondrial phospholipids in
386 health and diseases that lipids, unlike proteins and nucleic acids, have been stubbornly difficult to
387 visualize in cells, and "the next leap in the understanding of autophagic membrane dynamics
388 requires direct visualization of phospholipids in living cells to capture the transient
389 autophagosomes" (Hsu and Shi, 2017).

390 ***Could ApoL9 influence mitophagy?***

391 The fact that the PE-binding ability of ApoL9 is abolished by the deletion of a putative
392 transmembrane domain is directly indicative of the likelihood of the protein binding to PE embedded
393 in lipid bilayers/membranes. Localization to swollen mitochondria during treatment with brefeldin A
394 and bafilomycin A1 is also abolished in these deletion mutants ApoL9Δ111-123 and ApoL9Δ124-144.
395 Since the bulk of the PE in the cell is synthesised in the mitochondria by decarboxylation of
396 phosphatidylserine (Borkenhagen et al, 1961; Shiao et al., 1995), it is not surprising to find ApoL9 in
397 mitochondria (though it is not detected there in steady state conditions). The outer mitochondrial
398 membrane (OMM) is known to have a plethora of pro- and anti-apoptotic proteins of the Bcl-2
399 family that regulate mitochondrial integrity and physiology (Harris and Thompson 2000). We have
400 observed ApoL9 forming complete rings around mitochondria, and incomplete 'crescents' around
401 some (Fig. 2A, 2D, and S4.E), suggesting the possibility that ApoL9 molecules might gradually
402 colonize the mitochondrial membrane. This is reflected in a few images where the parts of the
403 membrane densely stained for TSPO are weakly stained for ApoL9, and vice versa **(Fig. S4.E)**. It is
404 common knowledge that autophagosomes are of different sizes depending on the cargo that is
405 targeted for degradation. For quite some time, it has been known that the mitochondria are one of
406 the various sources that contribute membrane to form autophagosomes by membrane addition

407 (Hailey et al., 2010; Cook et al., 2014). Cook et al. observed through electron microscopy that
408 mitochondrial membranes were sometimes contiguous with the membranes of the forming
409 autophagosome. Hailey et al. speculate about how the curvature-inducing property of PE at the
410 mitochondrial membrane, together with the hemifusion-inducing property of LC3, could potentially
411 be important to generate autophagosomes from mitochondria. They also note that during
412 autophagy, a significant quantity of membrane moves from autophagosomes to lysosomes through
413 fusion, and that PE comprises a large fraction of this. To the best of our knowledge, this study
414 reports the first instance of a PE-binding protein that has been observed localizing to mitochondria
415 synchronously with proteins of the autophagic machinery, and co-localizing with them. Another
416 connection worth noting is that ApoL9 has been reported to interact with PHB1 and PHB2 (Kreit et
417 al., 2015), two proteins of the inner mitochondrial membrane (IMM) that have been implicated in
418 controlling IMM organization by acting as protein and lipid scaffolds (Osman et al., 2009). Further,
419 PHB2 has been identified to function as a receptor for mitophagy on the IMM by bridging LC3 and
420 depolarized mitochondria whose outer membranes have ruptured (Wei et al., 2017). How ApoL9
421 could fit in this complex scheme of events is a topic for future study.

422 It has been reported (Maeda and Fadeel, 2014) that intact mitochondria could be expelled from
423 cells undergoing TNF-α-induced necroptosis and that this appeared to happen before the disruption
424 of the plasma membrane, suggesting an active mechanism of release. Several other reports have
425 also suggested that molecules derived from mitochondria and other organelles can act as DAMPs
426 (damage-associated molecular patterns) that act as signals for other cells in the immune system
427 (Krysko et al., 2011; Zhang et al., 2010). In our experiments, we have observed ApoL9-containing
428 ring-like structures being released from cells as early as 12 hours post bafilomycin A1 treatment, in
429 which period the cell membranes are unlikely to have suffered much damage from the actions of the
430 compound. Sun et al. (Sun et al., 2014) had reported that secretion of ApoL9a from cells can induce
431 epithelial proliferation, but commented that the mechanism of secretion was unclear. It would be
432 pertinent to investigate if ApoL9 can be secreted as part of the mitochondrial membrane in other
433 cell types. That the ApoLs are TNF-α-inducible genes points towards such a possibility.

434 ***Oligomerization of ApoL9***

435 Several cellular phenomena are regulated by proteins that oligomerize. This property might confer
436 additional advantages to proteins in certain conditions, such as improved stability, the ability to
437 concentrate molecules spatially, better interaction with partner proteins, and to assemble
438 complexes and scaffolds (Marianayagam et al., 2004). We can envisage a scenario where ApoL9, by
439 interacting with other ApoL9 molecules, can group together lipid molecules (PE) or proteins like

440 lipidated LC3 and concentrate them on discrete regions of the lipid bilayer on membranes of
441 autophagic vesicles, or organelles like lysosomes. Interorganellar contacts involving oligomerization
442 of ApoL9 could also be possible, for example between autophagosome-lysosome, or between
443 mitochondria. Several of the images of mitochondria show dense spots containing ApoL9 on the
444 membrane, and the mitochondria are also sometimes clustered together in apparent close contact
445 with each other, with the points of contact between mitochondria showing dense ApoL9 staining
446 (Fig. 2B, brefeldin). Though we do not know the significance of ApoL9 localizing to stress granules at
447 the moment, several proteins that are found in stress granules, e.g. TIA-1, TIAR, G3BP, etc. undergo
448 oligomerization with the help of some or other specific type of domain contained within them
449 (Tourriere et al., 2003; Gilks et al., 2004; Hua and Zhou, 2004).

450 The mutants ApoL9Δ111-123 and ApoL9Δ124-144 do not exhibit several of the properties displayed
451 by the wild type protein. Of the many properties of wild type ApoL9, association with mitochondria
452 and formation of insoluble curved structures seem to be the most likely properties linked with the
453 ability to bind PE, due to involvement of membrane/membrane fractions. At this stage, it is difficult
454 to comment on whether stress granule localization or microtubule binding depends on interaction
455 with lipid. However, oligomerization, interaction with GABARAP, and localization to aggresomes are
456 not directly linked to lipid-binding.

457 ***In what way could a lipid-binding MAP influence autophagy?***

458 The ability of ApoL9 to associate with microtubules might influence several cellular functions of the
459 protein, because it can potentially ferry lipid, or other, molecules to various parts of the cell while
460 attached to microtubules. Like several other MAPs (Itoh and Hotani, 1994), ApoL9 seems to stabilize
461 microtubules by binding to them, since mere overexpression of ApoL9 is sufficient for stabilized
462 microtubules to become visible in the cytoplasm. ApoL9 seems to be directly and strongly associated
463 with microtubules unlike proteins like LC3B that associate indirectly by virtue of their association
464 with other MAPs, since treatment of the B16F10^{LC3B} cell line with paclitaxel does not result in LC3B
465 becoming visible on stabilized microtubules in the cytoplasm **(Fig. S4.F)**. We could co-
466 immunoprecipitate α-tubulin with ApoL9, but since tubulin forms heterodimers further
467 investigations are needed to determine which tubulin types ApoL9 associates with and what the
468 structural details of the interaction are. It is interesting to observe that the helical region comprising
469 amino acids 54-70 that is a potential tubulin-binding motif lies exactly adjacent to FPRL, the potential
470 LIR motif of ApoL9 which when mutated reduced association with GABARAP by >50%. GABARAP
471 itself is a tubulin-binding protein, and it is not inconceivable that ApoL9 might simultaneously
472 associate with microtubules and GABARAP under certain conditions. Autophagosomes and

473 lysosomes are known to specifically travel along microtubules that undergo specific types of post-
474 translational modifications (Xie et al., 2010; Mohan et al., 2018); therefore it might be of interest to
475 investigate if ApoL9 localization is restricted to some or other subset of microtubules.

476 The identity of the highly curved, thread-like structures that accumulate in the cytoplasm after
477 prolonged treatment with bafilomycin A1 is unclear, as they did not co-localize with any protein or
478 organelle marker we used. Since their increase in the cell correlates with ApoL9 fractionating into a
479 Triton X-100-insoluble fraction of the lysate, it is possible that they comprise only ApoL9 and
480 membranous material. ApoL9 localizes to lysosomes on treatment with bafilomycin A1 or CQ, and
481 this property is not abolished in the non-PE-binding mutants suggesting that PE-binding is not
482 necessary for lysosomal localization. The C-terminus of ApoL9 contains the sequence YKTI, which
483 corresponds to a known consensus for lysosomal membrane targeting (YXXΦ) (Guarnieri et al.,
484 1993). ApoL9 seems to be targeted to lysosomes only under certain conditions, because in normal
485 conditions it doesn't seem to accumulate in these organelles. This points to the possibility of ApoL9
486 being involved in the later stages of autophagy, when autophagosomes mature and autolysosomes
487 come into play. The thread-like structures do not accumulate in cells expressing the non-PE-binding
488 mutants; it is likely that these structures are formed as a result of the prolonged downstream block
489 in the autophagic process due to the action of bafilomycin A1. It is widely accepted now that the
490 terminal step of autophagy is a process called autophagic lysosome reformation, in which a clathrin-
491 based budding mechanism facilitates the growth and elongation of tubules from autolysosomes
492 along microtubules, followed by scission of proto-lysosomes (Rong et al., 2012; Du et al., 2016).
493 However, it is still very unclear how different phospholipids regulate this mechanism, and how
494 lysosomal membrane and luminal proteins are sorted in this process. In our study, as mentioned
495 before, we have noticed a negative correlation between the presence of ApoL9 in juxtanuclear
496 lysosomes and in curved thread-like structures. We have also occasionally observed microtubule
497 proteins co-localizing with these structures. Therefore, we speculate that ApoL9, being a MAP and
498 an oligomerizing PE-binding protein, might regulate the formation of these or other similar tubules
499 from the lysosomes, thus potentially recycling membrane components for autophagy. It is
500 interesting to note that these ApoL9-positive curved, thread-like structures are seen only in
501 bafilomycin A1-treated cells but not in CQ-treated cells, and that the positioning of lysosomes in the
502 former case tends to be predominantly juxtanuclear. This may reflect the differences in the
503 mechanism of autophagy inhibition by these two compounds.

504 Taken together, the data presented in this study demonstrates that ApoL9 is a rather dynamic
505 protein that is found in several distinct compartments in the cell and interacts with various cellular

506 molecules. It is reasonable to speculate that it is involved in lipid transport in the cell and that its role
507 in autophagy is likely to be that of an adaptor protein. Since it is restricted to two species of rodents
508 and its expression levels are tissue-specific, it is unlikely to be an essential protein for autophagy and
509 we propose that it might confer some very selective advantage to rodent-specific metabolic
510 activities. One of the most significant differences between bigger and smaller animals is the high
511 metabolic rate per unit weight in the latter (Klieber, 1947). Assuming that ApoL9 has a small but not
512 insignificant contribution in augmenting a process such as protein homoeostasis or autophagy, and
513 considering its high levels in liver and brain tissue where autophagy plays critically important roles in
514 maintaining organ homoeostasis, it is possible to envisage a scenario where expression of such a
515 gene could confer a definite advantage to the fitness of a fast-metabolising species such as mouse.
516 Therefore we also feel that it would be appropriate if further investigations regarding ApoL9 be
517 performed in an *in vivo* context where its functions might be understood even better, like in hepatic
518 or neuronal tissues and in knockout mice.

519

520 ## MATERIALS AND METHODS

521 **Cell lines and reagents**

522 B16F10 mouse melanoma was obtained from the tissue culture facility, Dabur Research Foundation,
523 Ghaziabad, India. Mouse hepatoma H6 has been described (Thompson et al., 1981) and referenced
524 (Nandi et al., 1996) previously. HEK293T (ATCC® CRL 3216™) and HepG2 (ATCC® HB-8065™) were
525 gifts from Prof. Ganesh Nagaraju and Prof. Anjali Karande, Indian Institute of Science, Bangalore,
526 India. All cell lines were cultured in high glucose Dulbecco's Modified Eagle's Medium (DMEM)
527 containing 10% foetal bovine serum (FBS) and an antibiotic mixture comprising 10,000 units/mL
528 penicillin, 10,000 μg/mL streptomycin, and 25 μg/mL amphotericin B. The cell lines were maintained
529 in an incubator at 37˚C with 5% CO_2 and water provided for humidification. All cell lines were
530 routinely inspected for the absence of any potential contamination, including mycoplasma.

531 DMEM, FBS (E.U.-approved, South America origin), Earle's Balanced Salt Solution (EBSS), Opti-MEM
532 reduced serum medium, Antibiotic-Antimycotic solution (100X), Pierce BCA protein assay kit, and
533 PageRuler prestained protein ladder were purchased from Thermo Fisher Scientific, Waltham,
534 Massachusetts, USA. Trypsin (from porcine pancreas), puromycin dihydrochloride, Lipofectamine
535 2000, TRI reagent for RNA isolation, chloroquine, thapsigargin, paclitaxel, nocodazole, MG132, DTT
536 and 1,2-Dipalmitoyl-sn-glycero-3-phosphoethanolamine were purchased from Sigma-Aldrich, St.
537 Louis, Missouri, USA. H_20_2 and sodium arsenite were purchased from Merck, Darmstadt, Germany.

538 Bafilomycin A1 and brefeldin A were purchased from Cell Signaling Technology, Inc. (CST), Danvers,
539 Massachusetts, USA. Glutathione resin was purchased from G-Biosciences, St. Louis, Missouri.
540 Bovine albumin, fraction V, fatty acid-free was purchased from MP Biomedicals Ltd., Navi Mumbai,
541 Maharashtra, India. Amylose resin and all restriction endonucleases were procured from New
542 England Biolabs (NEB), Ipswich, Massachusetts, USA. All oligonucleotides used in PCR and cloning
543 were procured from Sigma-Aldrich. XT-20 high fidelity polymerase was used in all cloning protocols
544 and purchased from GeNei Pvt. Ltd., Bangalore, India. D (+) Maltose monohydrate was purchased
545 from HiMedia Laboratories Pvt. Ltd., Mumbai, India. Calf thymus DNA was procured from Amersham
546 plc, Buckinghamshire, United Kingdom. cOmplete™ protease inhibitor cocktail tablets, EDTA-free,
547 were purchased from Roche, Basel, Switzerland.

548 **Antibodies**

549 The following antibodies were used in this study: anti-V5 (mouse monoclonal, R960-25, Thermo
550 Fisher Scientific), anti-FLAG (mouse monoclonal, F1804, clone M2, Sigma-Aldrich), anti-LC3B (#2775,
551 rabbit polyclonal, CST), anti-β-actin (A3854, rabbit polyclonal, HRP-conjugate, Sigma-Aldrich), anti-V5
552 agarose affinity gel (A7345, monoclonal clone V5-10, Sigma-Aldrich), anti-eIF3η (sc-16377 (N20),
553 goat polyclonal, Santa Cruz Biotechnology, Inc., Dallas, Texas, USA), anti-GFP (sc-9996, mouse
554 monoclonal clone B2, Santa Cruz), anti-SQSTM1 (Ab56416, mouse monoclonal, Abcam, Cambridge,
555 United Kingdom), anti-V5 (V8137, rabbit polyclonal, Sigma-Aldrich), anti-LAMP1 (clone 1D4B, rat
556 monoclonal, Developmental Studies Hybridoma Bank, University of Iowa, Iowa, USA). Rabbit
557 polyclonal anti-MBP-ApoL9 antibody has been described and validated earlier in (Arvind and
558 Rangarajan, 2016). Also it should be noted that, in the bulk of experiments in the paper, ApoL9-V5
559 was detected in immunostaining and immunoblotting by anti-V5 antibody, unless specifically
560 mentioned otherwise.

561 **Plasmids and constructs**

562 The *Apol9a* gene was amplified as described earlier (Arvind and Rangarajan, 2016) from cDNA
563 prepared from total RNA of B16F10 cells treated with type I interferon. ORFs for other genes were
564 amplified from cDNA prepared from various mouse tissues/cell lines according to level of expression.
565 The *Apol9-V5* and *Apol9-3XFLAG* constructs were made by cloning the cDNAs into the XbaI and
566 HindIII sites in the vector *pBApo-EF1α pur* (Takara Bio Inc., Kusatsu, Shiga Prefecture, Japan). The V5
567 sequence was included in the reverse primer, while the 3XFLAG sequence was amplified from the
568 vector *p3XFLAG-CMV-10* (Sigma-Aldrich). The *MBP-ApoL9* construct was made by cloning *Apol9a*
569 amplified from the *Apol9-V5* construct and cloning into the SalI and HindIII sites in the vector *pMAL-*

570 *c2X* (NEB). MBP and MBP-ApoL9 were transformed into *E.coli BL21 (DE3)* competent cells and
571 purified according to the manufacturer's instructions. The inserts for *Lc3b* (BamHI/SalI), *Lc3a*
572 (EcoRI/SalI), *Gabarap* (BamHI/SalI), *Gabarapl1* (EcoRI/SalI), and *Gabarapl2* (EcoRI/SalI) were
573 amplified from cDNA derived from B16F10 melanoma cells and cloned in the vector *pGEX-4T-1* (GE
574 Healthcare, Chicago, Illinois, USA) into the sites indicated in parentheses. *Lc3b* was also cloned with
575 an N-terminal V5 tag into the BamHI and HindII sites of *pBApo-EF1α pur*. To create GFP-fusion
576 constructs *Lc3b* (EcoRI/BamHI) and *Gabarap* (HindIII/BamHI) were also cloned into the vector
577 *pEGFP-C1* (Clontech Laboratories, Mountain View, California, USA). N- and C-terminal GFP fusions of
578 ApoL9 were created by cloning *Apol9a* into *pEGFP-C1* (HindIII/KpnI) and *pEGFP-N1* (HindIII/ApaI)
579 respectively. The plasmid expressing GFP-tagged alpha tubulin was a gift from Prof. Vaishnavi
580 Ananthanarayanan, Centre for BioSystems Science and Engineering, IISc, Bangalore, India.
581 Translocator protein (*Tspo)* was cloned into the HindIII and BamHI sites of pEGFP-N1. *Tia-1* was
582 cloned into the EcoRI and BamHI sites of *p3XFLAG-CMV-10.*

583 **LIR mutants and deletion constructs**

584 LIR mutants of *Apol9-V5* were created by using complementary primers containing the desired
585 mutations in the region of the potential LIR, using wild type *Apol9-V5* to create amplicons with an
586 overlapping sequence, followed by overlap extension PCR to make the final mutant construct, and
587 cloning into the HindIII and XbaI sites of *pBApo-EF1α pur*.

588 Similarly, deletions in the *MBP-Apol9* sequence were made by using complementary primers
589 containing a deletion in the region of the desired deletion, followed by overlap extension PCR. The
590 constructs were cloned into the SalI and HindIII sites in the vector *pMAL-c2X*. The WT *MBP-Apol9*
591 construct was used as template for the initial rounds of PCR. To create *Apol9-V5 (Δ111-123)* and
592 *Apol9-V5 (Δ124-144)*, the inserts were amplified from the respective *MBP-Apol9* constructs and
593 cloned into the XbaI and HindIII sites of *pBApo-EF1α pur*. All clones were sequenced to confirm for
594 the desired mutations or deletions.

595 The various deletions are described and shown schematically **(Fig. S2.A,B)** .The N-terminal deletion
596 was 54 amino acids, spanning the full length of the helices in that region. The C-terminal deletion
597 was 30 amino acids in length which corresponded to a predicted coiled coil sequence in that region.
598 The BH3 deletion mutant encompassed amino acids 81-89, the core BH3 domain consensus
599 sequence. Based on predictions from software that predict transmembrane sequences in proteins
600 (Cserzo et al., 1997), two deletions were made that encompass potential transmembrane regions on
601 the ApoL9a sequence – amino acids 111-123, and 124-144. The other deletions were made randomly

602 in the remaining regions of the sequence, with no deletion exceeding an average length of 20-25
603 amino acids. Two exceptions were made based on exact stretches of 3 amino acids being present in
604 mouse PEBP1 and human PEBP4, respectively, both being proteins of the
605 phosphatidylethanolamine-binding protein family.

606 **Creation of cell lines stably expressing protein**

607 The B16F10 cell line stably expressing ApoL9 ($B16F10^{L9}$) has been described previously (Arvind and
608 Rangarajan, 2016). Briefly, the *ApoL9-V5* construct in *pBApo-EF1α pur* was linearized using ScaI and
609 transfected into semi-confluent B16F10 cells using Lipofectamine 2000. 48 h later, the cells were
610 subcultured into six-well plates and transformants were selected with 2 μg/mL puromycin. Ten days
611 later, single colonies were picked using sterile PYREX® cloning cylinders (6 mm x 8 mm, Corning Inc.,
612 Corning, New York, USA) and expanded into cultures in 6-well plates. The colonies were screened for
613 ApoL9 expression by indirect immunofluorescence using anti-V5 antibody, and clones with an
614 optimum level of expression were further expanded and frozen. $B16F10^{LC3B}$, $B16F10^{L9\Delta111-123}$ and
615 $B16F10^{L9\Delta124-144}$ were made by a similar procedure, using the *V5-LC3B*, *ApoL9-V5Δ111-123* and
616 *ApoL9-V5Δ124-144* constructs.

617 **Transfection procedures**

618 Lipofectamine 2000 was used according to the manufacturer's instructions. Electroporation was
619 done using Bio-Rad Gene Pulser™ electroporation cuvettes (0.4 cm gap; blue) and the Gene Pulser
620 Xcell™ electroporation system. Briefly, confluent B16F10 cells in a T75 culture flask were trypsinized
621 and centrifuged at 350 *g*. The cells were resuspended homogeneously in 2.5 mL Opti-MEM reduced
622 serum medium. 400 μL of cell suspension was mixed with 5-10 μg of plasmid DNA and ~20-30 μg of
623 sterile, sonicated calf thymus DNA, added to the cuvette and pulsed using the exponential decay
624 protocol at 240V and 950μF capacitance. The electroporated cell suspension was added to 1.2 mL
625 Opti-MEM in 35 mm culture dishes with or without glass cover slips. The medium was replaced with
626 fresh medium 4-6 h post electroporation, and the cells were processes for downstream experiments
627 16-24 h post transfection.

628 Calcium phosphate transfection was performed as described in (Sambrook and Russell, 2005) with
629 minor modifications. This technique was primarily used for HEK293T cells. Briefly, the growth
630 medium of cells (70% confluent) was replaced with 4 mL Opti-MEM just prior to transfection. For
631 transfection of a 60 mm dish, a cocktail was made that contained 8 μg plasmid DNA, ~30 μg calf
632 thymus DNA, and 22 μL of 2M $CaCl_2$ made up to 180 μL with water. To this, 180 μL of 2X Hepes-
633 buffered salt solution was added drop-wise with intermittent slow aeration by pipetting. The

634 mixture was incubated for 20 minutes and then added to the cells gently. The transfection medium
635 was replaced with fresh medium exactly 4 h post transfection, and the cells were processed for
636 downstream experiments ~24 hours after transfection.

637 **Cell lysis and protein estimation**

638 All cells were lysed in situ, i.e. by adding lysis buffer to the cell monolayer on the culture dishes and
639 incubating in a rocker at 4 ˚C. For making total cell lysates, RIPA buffer (50 mM Tris-HCl pH 7.4, 150
640 mM NaCl, 0.1% SDS, 0.5% sodium deoxycholate, 1% NP-40, 1 mM EDTA and complete protease
641 inhibitor cocktail) was used. The lysate was briefly sonicated to shear viscous DNA and centrifuged at
642 10,000 rpm at 4 ˚C in a tabletop microcentrifuge. The supernatant was used for western blotting. For
643 making Triton X-100 soluble and insoluble fractions of cell lysates, a lysis buffer comprising 50 mM
644 Tris-HCl pH 7.4, 150 mM NaCl, 1 mM EDTA and 0.1% Triton X-100 with protease inhibitor cocktails
645 was used. The pellet was resuspended in an appropriate volume of Laemmli buffer, after
646 centrifugation to clarify the lysate at 10,000 rpm at 4 ˚C on a microcentrifuge. The supernatant was
647 used for western blotting, pull-down, IP, or other experiments. All protein estimations were
648 performed using the Pierce BCA protein assay kit (Thermo Fisher Scientific).

649 **SDS-PAGE and western blotting**

650 SDS-PAGE gels were cast using a pre-made solution of acrylamide:bisacrylamide :: 29:1. Cell lysates
651 were loaded on gels, in most cases at 30 μg total protein per lane. The resolved proteins on the gels
652 were transferred to PVDF membranes (FluoroTrans® W, 0.2 μm pore size, Pall Corporation, New
653 York, USA) by semi-dry transfer at constant current. Recipes for separating and stacking gels, gel
654 running buffer and transfer buffer were standard recipes from (Green and Sambrook, 2014).
655 Membranes were blocked in 5% fat-free milk prepared in TBST (Tris-buffered saline with Tween 20;
656 50 mM Tris-HCl pH 8.0, 150 mM NaCl, 0.1% Tween 20). Primary antibodies were added according to
657 the concentration provided by the manufacturer (usually a dilution of 1: 1000 – 1: 5000), and
658 secondary HRP-conjugated antibodies were used at a dilution of 1: 10000. The blots were developed
659 using Immobilon® chemiluminescent HRP substrate (EMD Millipore, Merck), on an ImageQuant LAS
660 4000 platform (GE Healthcare). Quantitation of western blots was done using the software ImageJ,
661 and graphs were plotted using GraphPad Prism, version 6 (GraphPad Software, California, USA).
662 Blots were stripped using a buffer comprising 62.5 mM Tris-HCl pH 6.8, 2% SDS, and 100 mM 2-
663 mercaptoethanol, and re-probed for loading controls and other proteins.
664
665

666 **Protein pull-down and co-immunoprecipitation**

667 For GST/MBP pull-down assays, recombinant GST-fusion/MBP-fusion constructs were transformed
668 into BL21-DE3 *E. coli*, and glycerol stocks of colonies were made at a final concentration of 15%
669 glycerol. The cultures were inoculated into LB medium and induced with 0.5 mM IPTG for 3.5 h at
670 37˚C. After centrifugation, the pellets were lysed with a lysis buffer (20 mM Tris-HCl, 200 mM NaCl, 1
671 mM EDTA, pH 7.4, with added 1 mM PMSF). The solution was sonicated to lyse the cells and clarified
672 in a cold centrifuge at 10,000 *g*.

673 30-50 μL of affinity resin (amylose/glutathione agarose) was washed with the bacterial lysis buffer
674 twice, and the required quantity of bacterial lysate was added to it. The lysate was incubated on an
675 end-to-end rotator for binding for 30 min to 1 h, followed by three washes with wash buffer (lysis
676 buffer with a tiny amount of Triton X-100 for smooth movement of liquid in tube). Next, cell lysate
677 expressing/overexpressing the protein of interest was incubated with the beads for 2 h to overnight,
678 followed by three washes with wash buffer (mammalian cell lysis buffer). The beads were then
679 boiled in Laemmli buffer, centrifuged, and the supernatant was used for SDS-PAGE, followed by
680 western blotting. A fraction of the cell lysates used for IP was loaded as input. GST/MBP protein was
681 detected by staining the western blot membrane with a solution of 0.1% Ponceau S in 5% acetic acid
682 immediately after transfer.
683

684 **Indirect immunofluorescence**

685 Cells grown on acid-washed coverslips were fixed with 3.7% formaldehyde, washed twice with PBS,
686 and permeabilized with 0.1% Triton X-100 in PBS. After blocking with 5% BSA in PBS for 30 min., they
687 were incubated with primary antibodies in blocking solution for 2 hours. All antibodies were used at
688 1:200 dilution, except anti-LAMP1 (1:50). After 3 washes with PBS containing 0.05% Triton X-100,
689 they were incubated with secondary fluorophore-conjugated antibodies (Alexa Fluor 555/488;
690 Thermo Fisher Scientific/CST; 1:200 dilution) in blocking solution for 2 hours. After 3 more washes,
691 they were stained with 1μg/mL DAPI or Hoechst 33342, washed once, and mounted on a drop of
692 ProLong® series antifade reagents (Thermo Fisher Scientific).

693 Imaging was done on either of these platforms: Zeiss LSM 510, Zeiss LSM 880 with Airyscan, or Leica
694 TCS SP8 confocal microscopes. Intensity, brightness and colour contrast of images were balanced,
695 and scale bars were drawn, using either of the following software depending on which microscope
696 was used for imaging: LSM Image Browser or ZEN 2.3 Black (Carl Zeiss Microimaging), or Leica
697 Application Suite X ver. 3.4. Cropping, arranging and labelling of images were done using a

698 combination of Adobe Photoshop, Microsoft PowerPoint, and GNU Image Manipulation Program
699 (GIMP).
700
701 **Treatment of cells in culture**

702 Bafilomycin A1 and brefeldin A were dissolved in DMSO to make stock solutions of 100 μM and 10
703 mg/mL respectively. DMSO alone was used as a vehicle for treatment of cells in control dishes. For
704 all cell treatments, the addition of DMSO to cells never exceeded 0.1%. Chloroquine was dissolved in
705 water to make a 10 mM stock solution. Heat stress was applied by keeping cells in a CO_2 incubator
706 set at 43˚C for 30 min. Sodium arsenite was added to cells at 0.5 mM for 30 min. DTT was added to
707 the cells at 2 mM, from a freshly prepared stock solution in water. Thapsigargin was used at 500 nM
708 for 1 h, from a 1.5 mM stock solution in methanol. Bafilomycin A1 was used at 200 nM for
709 appropriate time periods, unless mentioned otherwise. Brefeldin A was used at 10 μg/mL.
710 Chloroquine was used at 50 μM. EBSS treatment of cells was done by washing the cells with EBSS
711 twice after removing the normal culture medium, and culturing in fresh EBSS for the stipulated time
712 periods. Paclitaxel was dissolved in DMSO to make a 10 mM stock and used to treat cells at 10 μM.
713 Nocodazole was dissolved in DMSO to make a 10 mg/mL stock and used to treat cells at 10 μg/mL.
714 MG132 was dissolved in DMSO to make a 10 mM stock and used to treat cells at 10 μM for 6 hours.
715 Cycloheximide was dissolved in water to make a 10 mg/mL stock and used at a concentration of 50
716 μg/mL in the chase assay.
717
718 **Protein-Lipid overlay assay**

719 MBP-ApoL9 and its deletion mutants were purified by binding cell lysates of IPTG-induced *E.coli*
720 cultures to amylose resin, eluted with 20mM maltose and quantified using a NanoDrop (Thermo
721 Fisher Scientific). They were electrophoresed on an SDS-PAGE to check for protein integrity. 1,2-
722 Dipalmitoyl-sn-glycero-3-phosphoethanolamine was dissolved in chloroform to 1 mg/mL and
723 warmed to dissolve fully. 1 μl of the solution was spotted on a nitrocellulose membrane (BioTrace™
724 NT, Pall Corporation) in quadruplicate and allowed to dry for 30 minutes. The membrane was
725 blocked in TBST containing 3% fatty acid-free BSA overnight, followed by incubation with the
726 respective purified MBP-fusion protein (2 μg/mL) for 2 h. After 3 washes in TBST, the membranes
727 were incubated with primary antibody (anti MBP-ApoL9 rabbit polyclonal) at 1:3000 dilution and
728 secondary antibody (goat anti-rabbit IgG-HRP) at 1:10000 in blocking solution and, as in the
729 procedure for western blotting, washed, coated with luminol substrate and viewed in a
730 chemiluminescence imager.

Acknowledgements

The staff of the Confocal/Bioimaging Facility, Division of Biological Sciences, Indian Institute of Science, are gratefully acknowledged for their assistance.

Competing Interests

The authors declare no competing interests.

Funding

This work was supported by J. C. Bose Fellowship grant SB/S2/JCB-025/2015 awarded by the Science and Engineering Research Board, Department of Science and Technology (DST), New Delhi, India (to P. N. R), and by the Department of Science and Technology Fund for Improvement of S&T Infrastructure in Higher Educational Institutions (DST-FIST) and University Grants Commission. P.N.R. also acknowledges the Department of Biotechnology (DBT)-Indian Institute of Science partnership program and research grants from DST and DBT.

References

Arvind, T. A. and Rangarajan, P. N. (2016). Mouse Apolipoprotein L9 is a phosphatidylethanolamine-binding protein. Biochemical and Biophysical Research Communications **479**, 636–642.

Birgisdottir, A., Lamark, T. and Johansen, T. (2013). The LIR motif – crucial for selective autophagy. Journal of Cell Science **126**, 3237-3247.

Borkenhagen, L., Kennedy, E., and Fielding, L. (1961). Enzymatic Formation and Decarboxylation of Phosphatidylserine. Journal of Biological Chemistry **236**, PC28-PC30.

Cook, K. L., Soto-Pantoja, D. R., Abu-Asab, M., Clarke, P. A., Roberts, D. D. and Clarke, R. (2014). Mitochondria directly donate their membrane to form autophagosomes during a novel mechanism of parkin-associated mitophagy. Cell & Bioscience **4**, 16.

Cserzo, M., Wallin, E., Simon, I., Heijne, G. V. and Elofsson, A. (1997). Prediction of transmembrane alpha-helices in prokaryotic membrane proteins: the dense alignment surface method. Protein Engineering Design and Selection **10**, 673–676.

Dall'Armi, C., Devereaux, K. A. and Di Paolo, G. (2013). The Role of Lipids in the Control of Autophagy. Current Biology **23**, R33–R45.

Du, W., Su, Q. P., Chen, Y., Zhu, Y., Jiang, D., Rong, Y., Zhang, S., Zhang, Y., Ren, H., Zhang, C., et al. (2016). Kinesin 1 Drives Autolysosome Tubulation. Developmental Cell **37**, 326–336.

Fujiwara, T., Oda, K., Yokota, S., Takatsuki, A. and Ikehara, Y. (1988). Brefeldin A Causes Disassembly of the Golgi Complex and Accumulation of Secretory Proteins in the Endoplasmic Reticulum. Journal of Biological Chemistry **263**, 18545-18552.

Gilks, N., Kedersha, N., Ayodele, M., Shen, L., Stoecklin, G., Dember, L. M. and Anderson, P. (2004). Stress Granule Assembly Is Mediated by Prion-like Aggregation of TIA-1. Molecular Biology of the Cell **15**, 5383–5398.

Green, M. R. and Sambrook, J. (2014). Molecular cloning: a laboratory manual. Cold Spring Harbor, NY: Cold Spring Harbor Laboratory Press.

Guarnieri, F., Arterburn, L., Penno, M., Cha, Y. and August, J. T. (1993). Journal of Biological Chemistry **268**, 1941-1946.

785 Hailey, D. W., Rambold, A. S., Satpute-Krishnan, P., Mitra, K., Sougrat, R., Kim, P. K. and Lippincott-
786 Schwartz, J. (2010). Mitochondria Supply Membranes for Autophagosome Biogenesis during
787 Starvation. Cell **141**, 656–667.

788 Harris, M. H. and Thompson, C. B. (2000). The role of the Bcl-2 family in the regulation of outer
789 mitochondrial membrane permeability. Cell Death & Differentiation **7**, 1182–1191.

790 Hsu, P. and Shi, Y. (2017). Regulation of autophagy by mitochondrial phospholipids in health and
791 diseases. Biochimica et Biophysica Acta (BBA) - Molecular and Cell Biology of Lipids **1862**, 114–129.

792 Hua, Y. and Zhou, J. (2004). Survival motor neuron protein facilitates assembly of stress
793 granules. FEBS Letters **572**, 69–74.

794 Itoh, T. J. and Hotani, H. (1994). Microtubule-Stabilizing Activity of Microtubule-Associated Proteins
795 (MAPs) Is Due to Increase in Frequency of Rescue in Dynamic Instability: Shortening Length
796 Decreases with Binding of MAPs onto Microtubules. Cell Structure and Function **19**, 279–290.

797 Kabeya, Y. (2000). LC3, a mammalian homologue of yeast Apg8p, is localized in autophagosome
798 membranes after processing. The EMBO Journal **19**, 5720–5728.

799 Kabeya, Y. (2004). LC3, GABARAP and GATE16 localize to autophagosomal membrane depending on
800 form-II formation. Journal of Cell Science **117**, 2805–2812.

801 Kale, J., Osterlund, E. J. and Andrews, D. W. (2018). BCL-2 family proteins: changing partners in the
802 dance towards death. Cell Death & Differentiation **25**, 65–80.

803 Kleiber, M. (1947). Body Size And Metabolic Rate. Physiological Reviews **27**, 511–541.

804 Kreit, M., Paul, S., Knoops, L., Cock, A. D., Sorgeloos, F. and Michiels, T. (2014). Inefficient Type I
805 Interferon-Mediated Antiviral Protection of Primary Mouse Neurons Is Associated with the Lack of
806 Apolipoprotein L9 Expression. Journal of Virology **88**, 3874–3884.

807 Kreit, M., Vertommen, D., Gillet, L. and Michiels, T. (2015). The Interferon-Inducible Mouse
808 Apolipoprotein L9 and Prohibitins Cooperate to Restrict Theiler's Virus Replication. Plos One **10**(7).

809 Krysko, D. V., Agostinis, P., Krysko, O., Garg, A. D., Bachert, C., Lambrecht, B. N. and Vandenabeele,
810 P. (2011). Emerging role of damage-associated molecular patterns derived from mitochondria in
811 inflammation. Trends in Immunology **32**, 157–164.

812 Lee, S. A., Kim, Y. J. and Lee, C. S. (2013). Brefeldin A Induces Apoptosis by Activating the
813 Mitochondrial and Death Receptor Pathways and Inhibits Focal Adhesion Kinase-Mediated Cell
814 Invasion. Basic & Clinical Pharmacology & Toxicology **113**, 329-338.

815 Maeda, A. and Fadeel, B. (2014). Mitochondria released by cells undergoing TNF-α-induced
816 necroptosis act as danger signals. Cell Death & Disease **5**, e1312.

817 Marianayagam, N. J., Sunde, M. and Matthews, J. M. (2004). The power of two: protein dimerization
818 in biology. Trends in Biochemical Sciences **29**, 618–625.

819 Mauthe, M., Orhon, I., Rocchi, C., Zhou, X., Luhr, M., Hijlkema, K.-J., Coppes, R. P., Engedal, N., Mari,
820 M. and Reggiori, F. (2018). Chloroquine inhibits autophagic flux by decreasing autophagosome-
821 lysosome fusion. Autophagy **14**, 1435–1455.

822 Mauvezin, C., Nagy, P., Juhász, G. and Neufeld, T. P. (2015). Autophagosome–lysosome fusion is
823 independent of V-ATPase-mediated acidification. Nature Communications **6**: 7007.

824 Mohan, N., Sorokina, E. M., Verdeny, I. V., Alvarez, A. S. and Lakadamyali, M. (2018). Detyrosinated
825 microtubules spatially constrain lysosomes facilitating lysosome–autophagosome fusion. The Journal
826 of Cell Biology **218**, 632–643.

827 Monajemi, H., Fontijn, R. D., Pannekoek, H. and Horrevoets, A. J. (2002). The Apolipoprotein L Gene
828 Cluster Has Emerged Recently in Evolution and Is Expressed in Human Vascular Tissue. Genomics **79**,
829 539–546.

830 Nandi, D., Jiang, H. and Monaco, J.J. (1996). Identification of MECL-1 (LMP-10) as the Third
831 IFN-γ -inducible Proteasome Subunit. Journal of Immunology **156**, 2361-2364.

832 Nath, S., Dancourt, J., Shteyn, V., Puente, G., Fong, W. M., Nag, S., Bewersdorf, J., Yamamoto, A.,
833 Antonny, B. and Melia, T. J. (2014). Lipidation of the LC3/GABARAP family of autophagy proteins
834 relies on a membrane-curvature-sensing domain in Atg3. Nature Cell Biology **16**, 415–424.

835 Niu, T.-K., Pfeifer, A. C., Lippincott-Schwartz, J. and Jackson, C. L. (2005). Dynamics of GBF1, a
836 Brefeldin A-Sensitive Arf1 Exchange Factor at the Golgi. Molecular Biology of the Cell **16**, 1213–1222.

837 Osman, C., Haag, M., Potting, C., Rodenfels, J., Dip, P. V., Wieland, F. T., Brügger, B., Westermann, B.
838 and Langer, T. (2009). The genetic interactome of prohibitins: coordinated control of cardiolipin and
839 phosphatidylethanolamine by conserved regulators in mitochondria. The Journal of Cell Biology **184**,
840 583–596.

841 Rong, Y., Liu, M., Ma, L., Du, W., Zhang, H., Tian, Y., Cao, Z., Li, Y., Ren, H., Zhang, C., et al. (2012).
842 Clathrin and phosphatidylinositol-4,5-bisphosphate regulate autophagic lysosome
843 reformation. Nature Cell Biology **14**, 924–934.

844 Sambrook, J. & Russell, D.W (eds.) (2005).Calcium phosphate–mediated transfection of eukaryotic
845 cells (2005). Nature Methods **2**, 319–320.
846

847 Shatz, O., Holland, P., Elazar, Z. and Simonsen, A. (2016). Complex Relations Between Phospholipids,
848 Autophagy, and Neutral Lipids. Trends in Biochemical Sciences **41**, 907–923.

849 Shiao, Y., Lupo, G. and Vance, J. (1995). Evidence that phosphatidylserine is imported into
850 mitochondria via a mitochondria-associated membrane and that the majority of mitochondrial
851 phosphatidylethanolamine is derived from decarboxylation of phosphatidylserine. Journal of
852 Biological Chemistry **270**, 11190–11198

853 Sun, L., Miyoshi, H., Origanti, S., Nice, T. J., Barger, A. C., Manieri, N. A., Fogel, L. A., French, A. R.,
854 Piwnica-Worms, D., Piwnica-Worms, H., et al. (2015). Type I Interferons Link Viral Infection to
855 Enhanced Epithelial Turnover and Repair. Cell Host & Microbe **17**, 85–97.

856 Teplova, V. V., Tonshin, A. A., Grigoriev, P. A., Saris, N.-E. L. and Salkinoja-Salonen, M. S. (2007).
857 Bafilomycin A1 is a potassium ionophore that impairs mitochondrial functions. Journal of
858 Bioenergetics and Biomembranes **39**, 321–329.

859 Thompson, E. A., Keith, R. H., Cavanaugh, A. H. and Wood, K. M. (1981). The relationship between
860 the activity of DNA-dependent RNA polymerase I and the rate of synthesis of rRNA in hepatoma cells
861 in culture. Biochemical Journal **194**, 43–51.

862 Tourriere, H., Gallouzi, I.-E., Chebli, K., Capony, J. P., Mouaikel, J., Geer, P. V. D. and Tazi, J. (2001).
863 RasGAP-Associated Endoribonuclease G3BP: Selective RNA Degradation and Phosphorylation-
864 Dependent Localization. Molecular and Cellular Biology **21**, 7747–7760.

865 Wang, H. and Olsen, R. W. (2002). Binding of the GABAA Receptor-Associated Protein (GABARAP) to
866 Microtubules and Microfilaments Suggests Involvement of the Cytoskeleton in GABARAPGABAA
867 Receptor Interaction. Journal of Neurochemistry **75**, 644–655.

868 Wei, Y., Chiang, W.-C., Sumpter, R., Mishra, P. and Levine, B. (2017). Prohibitin 2 Is an Inner
869 Mitochondrial Membrane Mitophagy Receptor. Cell **168,** 224-238.

870 Wild, P., Mcewan, D. G. and Dikic, I. (2013). The LC3 interactome at a glance. Journal of Cell
871 Science **127**, 3–9.

872 Xie, R., Nguyen, S., Mckeehan, W. L. and Liu, L. (2010). Acetylated microtubules are required for
873 fusion of autophagosomes with lysosomes. BMC Cell Biology **11**:89.

874 Zhang, Q., Raoof, M., Chen, Y., Sumi, Y., Sursal, T., Junger, W., Brohi, K., Itagaki, K. and Hauser, C.
875 J. (2010). Circulating mitochondrial DAMPs cause inflammatory responses to injury. Nature **464**,
876 104–107.

877 Zhaorigetu, S., Yang, Z., Toma, I., Mccaffrey, T. A. and Hu, C.-A. A. (2011). Apolipoprotein L6, Induced
878 in Atherosclerotic Lesions, Promotes Apoptosis and Blocks Beclin 1-dependent Autophagy in
879 Atherosclerotic Cells. Journal of Biological Chemistry **286**, 27389–27398.

Figure 1

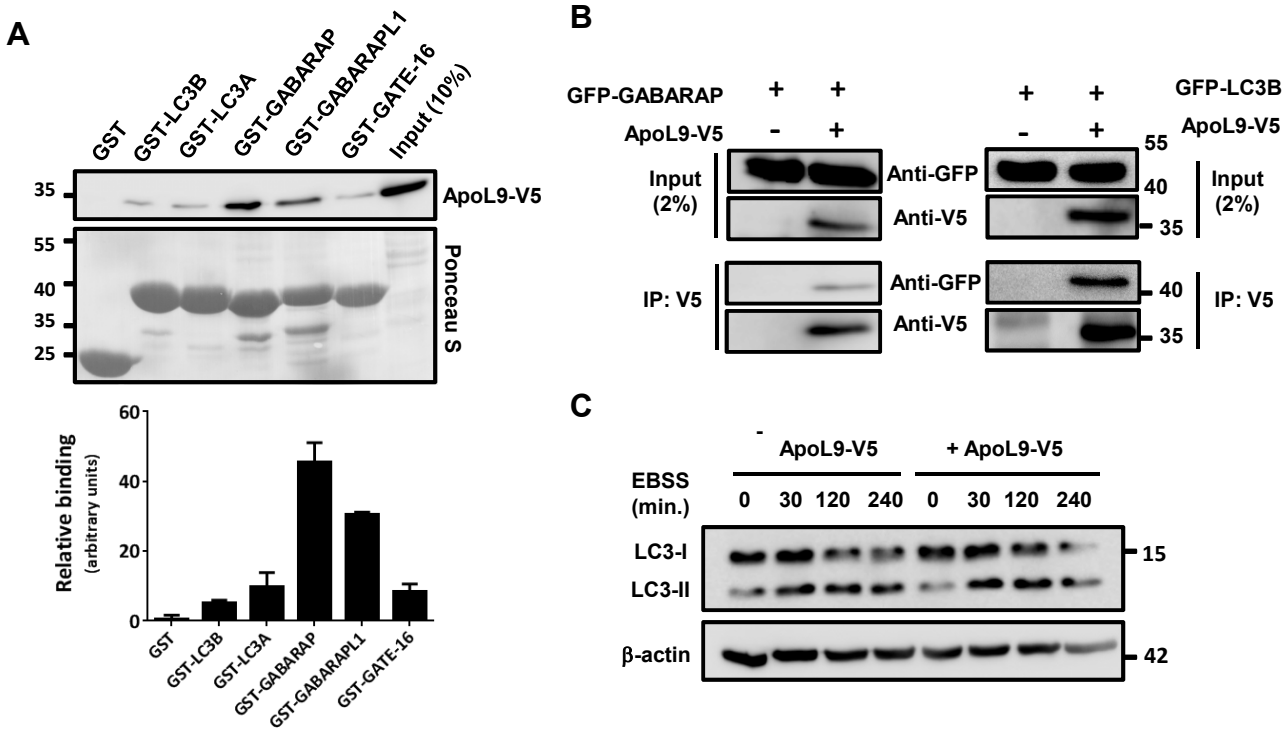

Fig.1: **ApoL9 interacts with proteins of the LC3 and GABARAP subfamilies**

A. Interaction of ApoL9-V5 expressed in HEK293T cells with recombinant GST-tagged proteins of the LC3 and GABARAP subfamilies. GST served as a negative control. GST-fusion proteins were stained by Ponceau S. Quantification of binding is shown in the graph below. Values represent mean ± s.d.; n=3. **B.** Co-immunoprecipitation of GFP-tagged LC3B and GABARAP with ApoL9-V5, from lysates of HEK293T cells transfected with *ApoL9-V5* and either of the GFP-fusions, by anti-V5 agarose affinity gel. Cells transfected with control vector and *GFP-Gabarap/GFP-Lc3b* served as negative controls. 2% of the total quantity of protein lysate taken for IP served as input to confirm efficient transfection. **C.** Comparison of LC3-I and LC3-II levels in HEK293T cells expressing (lanes 5-8) and not expressing (lanes 1-4) ApoL9-V5. *Apol9-V5* was transfected into cells by the calcium phosphate method. Cells transfected with empty vector (insert-less *pBApo -EF1α pur*) served as control. β-actin was used as a loading control.

Figure 2

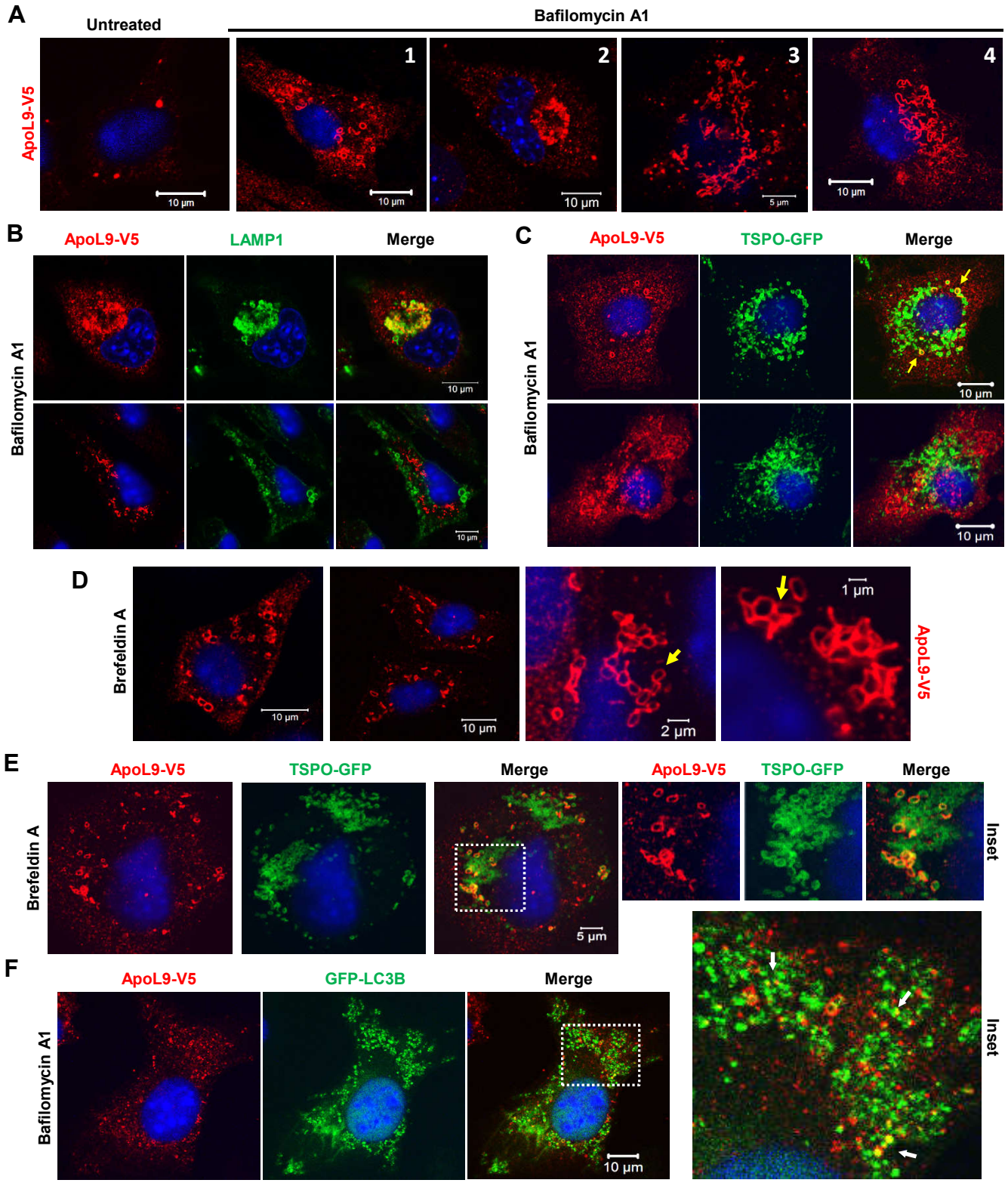
A
Untreated
Bafilomycin A1
ApoL9-V5
1
2
3
4
10 µm
5 µm
B
ApoL9-V5
LAMP1
Merge
Bafilomycin A1
C
ApoL9-V5
TSPO-GFP
Merge
Bafilomycin A1
D
Brefeldin A
1 µm
2 µm
ApoL9-V5
E
ApoL9-V5
TSPO-GFP
Merge
Brefeldin A
Inset
5 µm
F
ApoL9-V5
GFP-LC3B
Merge
Bafilomycin A1
Inset

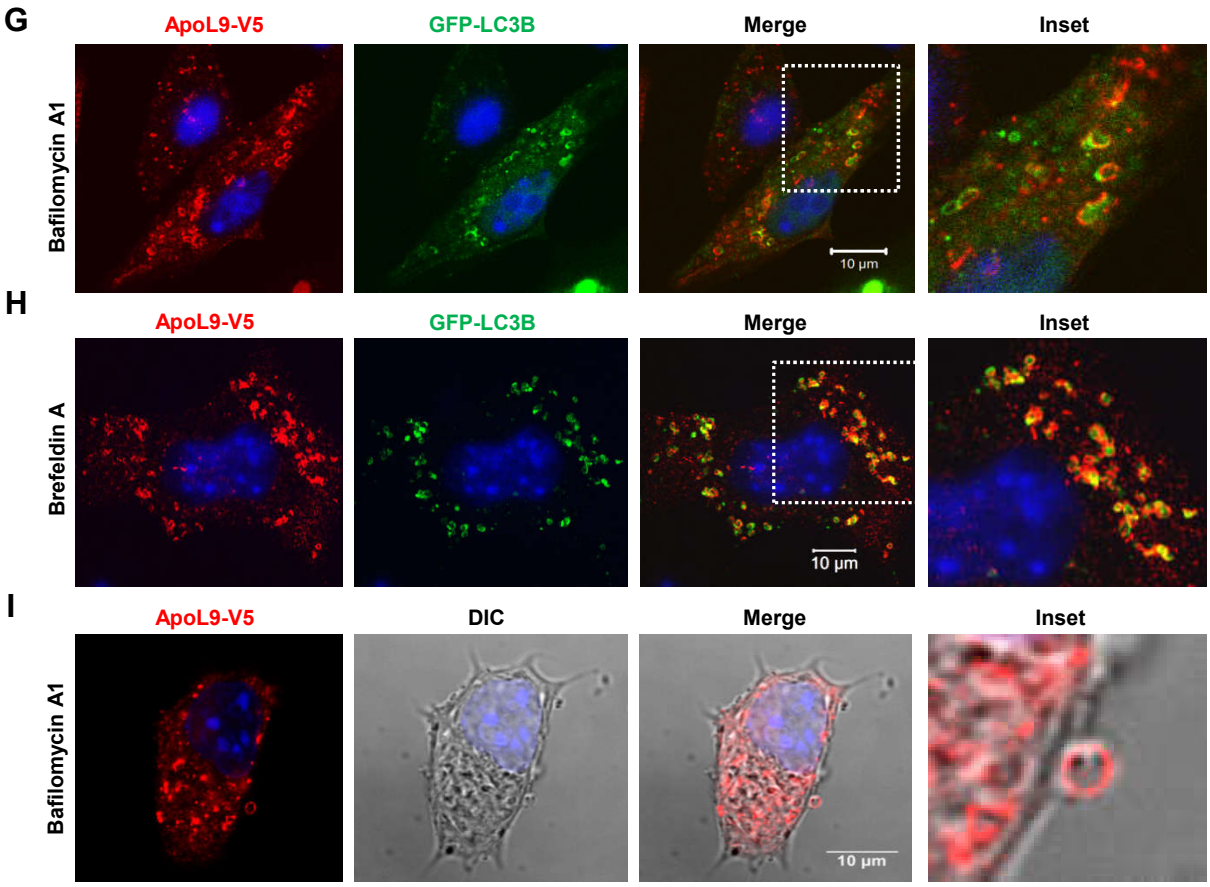

Fig.2: Subcellular distribution of ApoL9 after treatment with bafilomycin A1 and brefeldin A

A. Patterns of distribution of ApoL9-V5 in various cells of B16F10^{L9} after treatment with 200 nM bafilomycin A1 for 10-18 h, showing: ring-shaped structures (1), accumulation in the juxtanuclear region (2), and curved, thread-like structures (3, 4). Anti-V5 antibody was used to detect ApoL9. **B.** Indirect immunofluorescence for ApoL-V5 and lysosomal marker LAMP1 in B16F10^{L9} cells treated with bafilomycin A1 for 12 h, showing co-localization in the juxtanuclear region (upper panel). ApoL9 in curved, thread-like structures (lower panel) does not co-localize with LAMP1. Anti-V5 and anti-LAMP1 antibodies were used. **C.** Indirect immunofluorescence for ApoL9 and outer mitochondrial membrane (OMM) marker TSPO in B16F10^{L9}cells treated with bafilomycin A1 for 12 h, showing co-localization of ApoL9-V5-positive rings with TSPO-GFP (upper panel, yellow arrows). ApoL9-V5 in curved, thread-like structures (lower panel) does not co-localize with TSPO-GFP. *Tspo-GFP* was electroporated into B16F10^{L9} cells. **D.** Patterns of distribution of ApoL9-V5 in various cells after treatment with 10 mg/mL brefeldin A for 14-18 h. Note the proximity between ring-shaped structures (yellow arrows) in images of higher magnification. **E.** Indirect immunofluorescence for ApoL9-V5 and TSPO-GFP in B16F10^{L9} cells treated with brefeldin A, and (right) magnified inset. Note that only a fraction of the mitochondria are positive for ApoL9. **F.** A B16F10^{L9} cell electroporated with the *GFP-Lc3b* construct and treated with bafilomycin A1 for 12 h, showing GFP-LC3B on punctate autophagosomes. ApoL9-V5 is not present on autophagosomes, but partial co-localization is visible in a few places (magnified boxed inset; white arrows). **G-H.** Images showing GFP-LC3B (transfected by electroporation) in the vicinity of ApoL9-containing mitochondria in B16F10^{L9} cells treated with bafilomycin A1 and brefeldin A, respectively. Boxed insets are magnified. **I.** An ApoL9-positive ring-shaped vesicle exiting the cell boundary. B16F10^{L9} cells were treated with bafilomycin A1 for 16h.

Figure 3

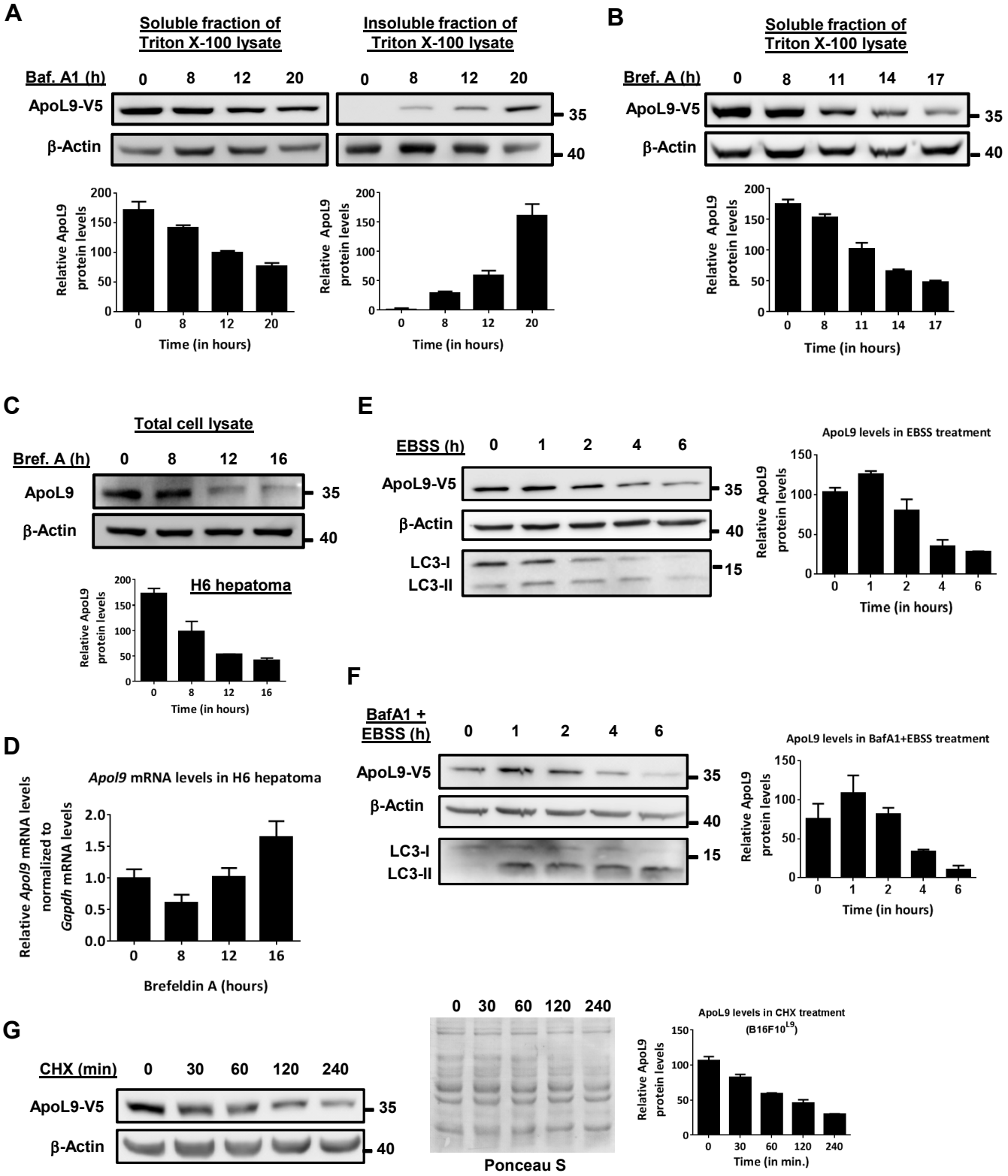
A
Soluble fraction of Triton X-100 lysate
Insoluble fraction of Triton X-100 lysate
Baf. A1 (h)
0 8 12 20
ApoL9-V5
β-Actin
35
40
Relative ApoL9 protein levels
Time (in hours)
B
Soluble fraction of Triton X-100 lysate
Bref. A (h)
0 8 11 14 17
C
Total cell lysate
Bref. A (h)
0 8 12 16
ApoL9
H6 hepatoma
D
Apol9 mRNA levels in H6 hepatoma
Relative Apol9 mRNA levels normalized to Gapdh mRNA levels
Brefeldin A (hours)
E
EBSS (h)
0 1 2 4 6
LC3-I
LC3-II
15
ApoL9 levels in EBSS treatment
F
BafA1 + EBSS (h)
ApoL9 levels in BafA1+EBSS treatment
G
CHX (min)
0 30 60 120 240
Ponceau S
ApoL9 levels in CHX treatment (B16F10L9)
Time (in min.)

Fig.3: Effect of treatment with various compounds on ApoL9 protein levels in the cell

A. Immunoblotting for ApoL9-V5 in Triton X-100-soluble and insoluble fractions of B16F10^{L9}cells treated with bafilomycin A1 for the indicated time periods, and (below) quantification of the blots. **B.** Immunoblotting for ApoL9-V5 in the Triton X-100-soluble fraction of B16F10^{L9} cells treated with brefeldin A for the indicated time periods and (below) quantification. No ApoL9 was detected in the Triton X-100-insoluble fraction. **C.** Immunoblotting for endogenous ApoL9 in hepatoma H6 treated with brefeldin A for the indicated time periods and (below) quantification. Anti-MBP-ApoL9 antibody was used to detect ApoL9. **D.** qPCR for *Apol9* mRNA levels in hepatoma H6 treated with brefeldin A for the same time periods as in C., normalized to *Gapdh*. Error bars indicate mean ± s.d (n=3). **E-F.** Immunoblotting for ApoL9-V5 in B16F10^{L9} cells treated with EBSS alone, or EBSS+ 400 nM bafilomycin A1, for the indicated time periods. Blots were stripped and reprobed with anti-LC3B antibody to confirm the effect of autophagy inhibition. Blots are quantified and represented as graphs (right). **G.** Immunoblotting for ApoL9-V5 in B16F10^{L9} cells after treatment with 50 mg/mL cycloheximide (CHX) for the indicated time periods and (far right) quantification of the blot. The blot is stained with Ponceau S to show loading.

Figure 4

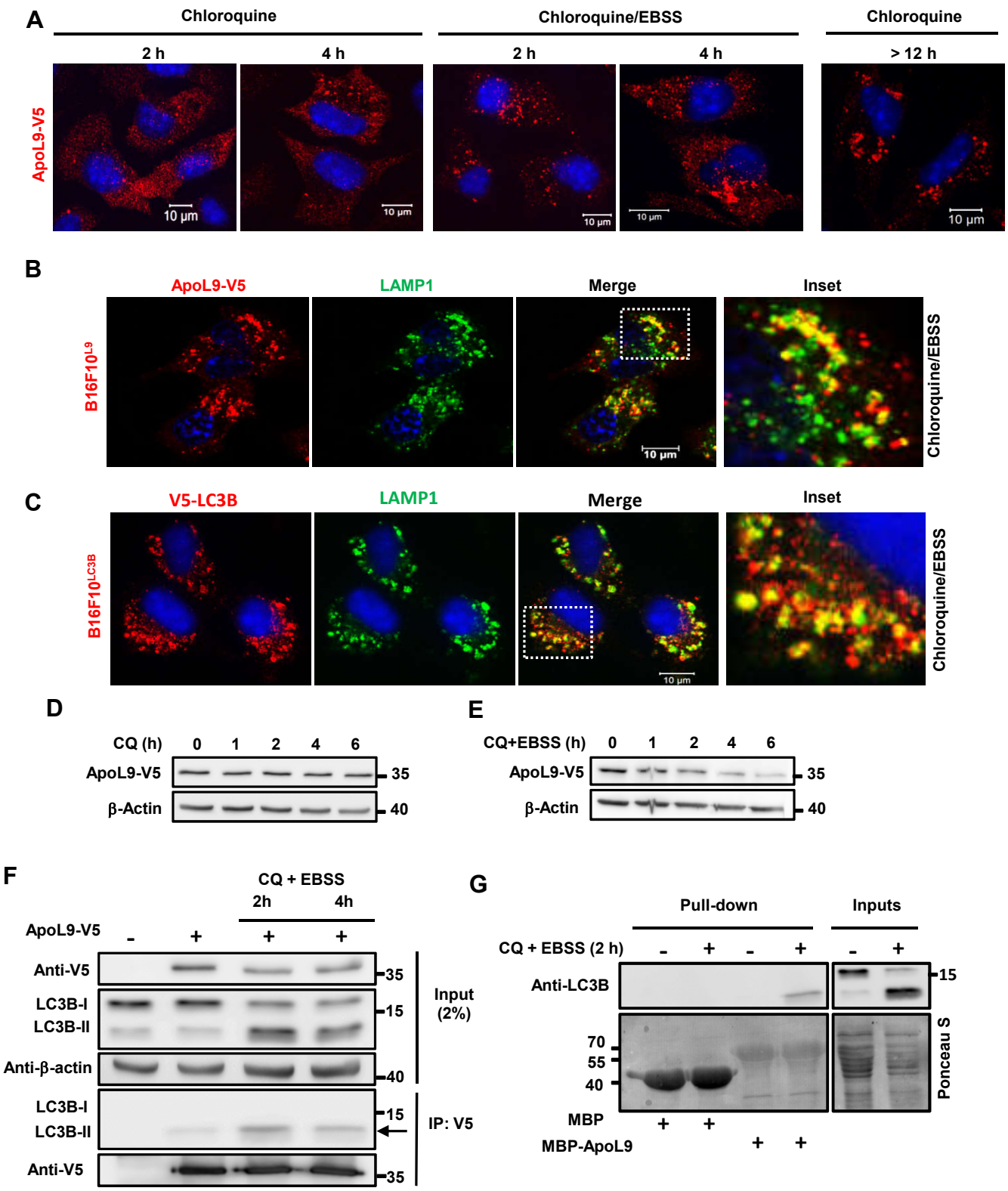
A
Chloroquine
Chloroquine/EBSS
Chloroquine
2 h
4 h
2 h
4 h
> 12 h
ApoL9-V5
10 µm
B
ApoL9-V5
LAMP1
Merge
Inset
B16F10L9
Chloroquine/EBSS
C
V5-LC3B
LAMP1
Merge
Inset
B16F10LC3B
Chloroquine/EBSS
D
CQ (h) 0 1 2 4 6
ApoL9-V5
β-Actin
35
40
E
CQ+EBSS (h) 0 1 2 4 6
ApoL9-V5
β-Actin
35
40
F
CQ + EBSS
2h 4h
ApoL9-V5 - + + +
Anti-V5
LC3B-I
LC3B-II
Anti-β-actin
Input (2%)
35
15
40
LC3B-I
LC3B-II
Anti-V5
IP: V5
15
35
G
Pull-down
Inputs
CQ + EBSS (2 h) - + - + - +
Anti-LC3B
15
70
55
40
Ponceau S
MBP + +
MBP-ApoL9 + +

Fig.4: Effect of treatment with chloroquine on ApoL9 in B16F10^{L9} cells

A. Subcellular distribution of ApoL9-V5 in B16F10^{L9} cells cultured with 50 mM CQ, or 50 mM CQ+EBSS, for the indicated time periods. Note the heavier aggregation pattern in CQ+EBSS compared with CQ for the same time period. **B, C.** Indirect immunofluorescence for LAMP1 in B16F10^{L9} and B16F10^{LC3B} cells respectively after treatment with CQ+EBSS for 4 h. Note the similar patterns but higher degree of co-localization of LC3B with LAMP1. Boxed insets are magnified on the right. **D, E.** ApoL9-V5 protein levels in B16F10^{L9} cells cultured with CQ alone, or CQ+EBSS, for the indicated time points and (below) quantification. **F.** Co-immunoprecipitation of endogenous LC3B with ApoL9-V5 by anti-V5 agarose from lysates of HEK293T cells transfected with *Apol9-V5* and treated with CQ+EBSS (lanes 3, 4). Lane 1 is cells transfected with control vector, while lane 2 is untreated cells. Note the selective immunoprecipitation of LC3-II in lanes 2-4 (arrow). Anti-LC3B antibody was used. **G.** Pulldown of LC3B from cell lysates of HEK293T cells treated (lanes 2, 4) or not treated (lanes 1, 3) with CQ+EBSS by recombinant MBP/MBP-ApoL9 bound to amylose resin. Blots were stained with Ponceau S to visualize input and recombinant proteins.

Figure 5

A

Mutation of residues		
Original	Mutated	Position
1. YSLV	ASLA	8-11
2. FLKV	ALKA	63-66
3. FPRL	APRA	67-70
4. WSDV	ASDA	264-267
5. YKTI	AKTA	307-310

B

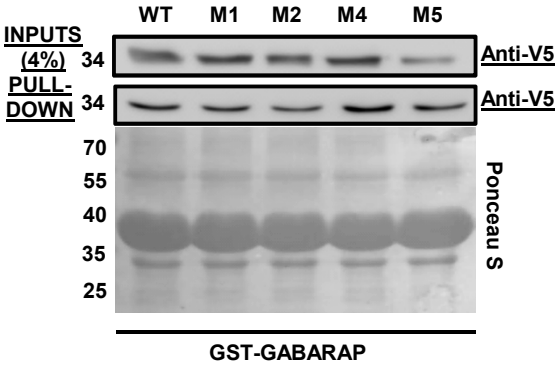

C

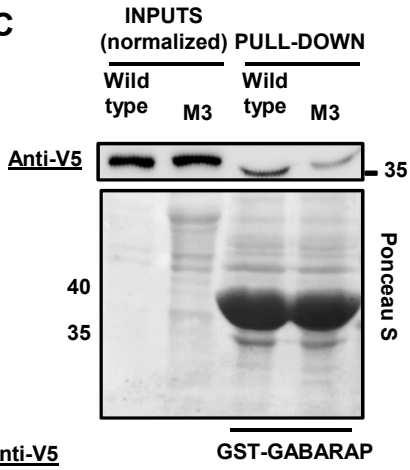

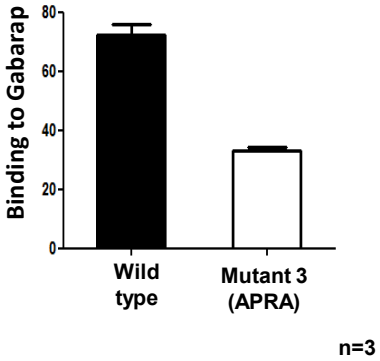

D

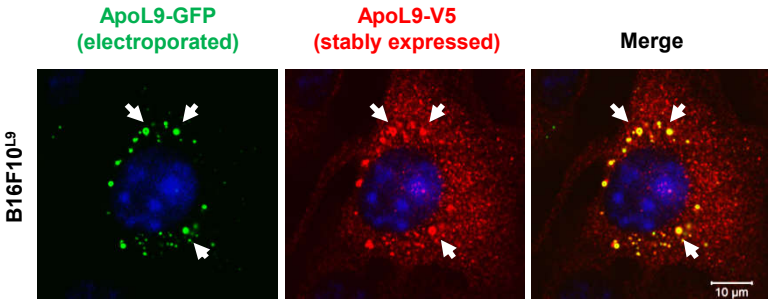

E

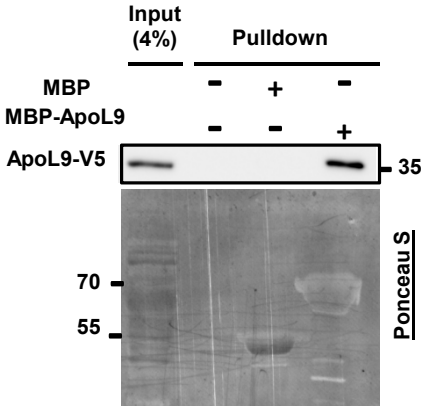

F

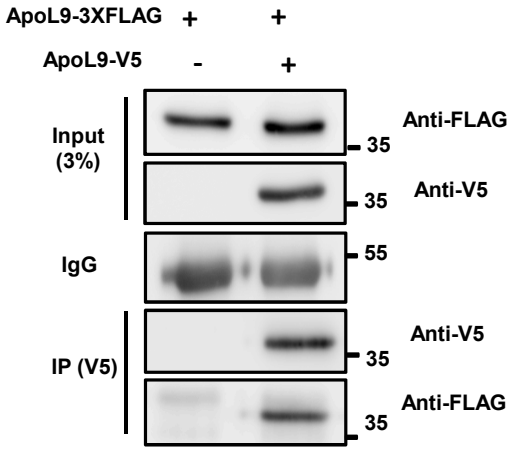

G

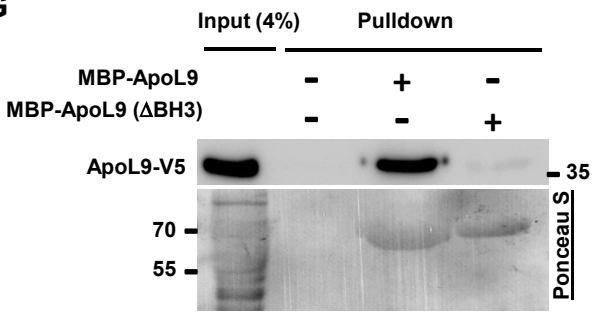

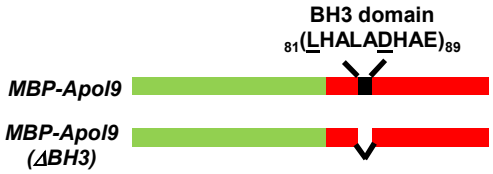

Fig.5: LIR mutants, and oligomerization of ApoL9

A. The five potential LIRs, their mutated versions, and their positions in the ApoL9 protein sequence. The mutant forms of the protein were named M1, M2 … M5. **B.** Pull-down of LIR mutants M1, M2, M4 and M5 of ApoL9-V5 (HEK293T) by recombinant GST-GABARAP (from *E.coli*), similar to Fig. 1A. **C.** Comparison of pull-down of WT ApoL9-V5 and LIR mutant M3 by GST-GABARAP, and quantification of binding (mean ± s.d. ; n=3) **D.** Altered subcellular distribution pattern of ApoL9-V5 in B16F10^{L9} cells electroporated with ApoL9-GFP (compare with untreated ApoL9-V5 in Fig. 7D/8A). White arrows help visualize similarity in patterns. **E.** Pull-down of ApoL9-V5 from transfected HEK293T cells by recombinant MBP/MBP-ApoL9 bound to amylose resin. Note that only MBP-ApoL9 is able to pull down ApoL9-V5. **F.** Coimmunoprecipitation of ApoL9-3XFLAG with ApoL9-V5 by anti-V5 agarose, from lysates of HEK293T cells transfected with both constructs. Cells transfected with control vector and ApoL9-3XFLAG served as a negative control. **G.** Pull-down of ApoL9-V5 (HEK293T) by recombinant MBP-ApoL9 and MBP-ApoL9 (ΔBH3). A schematic of the BH3 domain deletion is shown on the right.

Figure 6

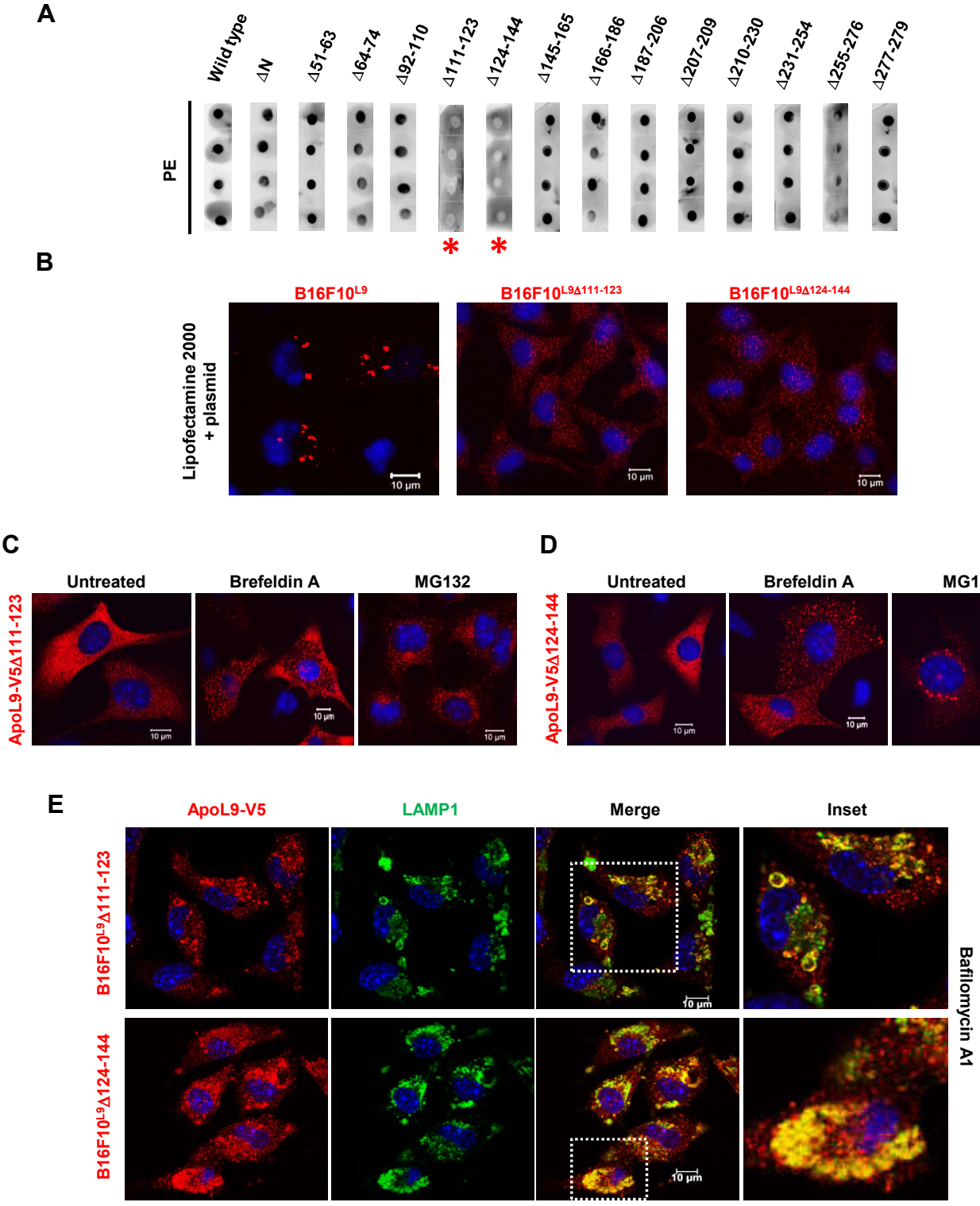
A
Wild type
ΔN
Δ51-63
Δ64-74
Δ92-110
Δ111-123
Δ124-144
Δ145-165
Δ166-186
Δ187-206
Δ207-209
Δ210-230
Δ231-254
Δ255-276
Δ277-279
PE
*
*
B
B16F10L9
B16F10L9Δ111-123
B16F10L9Δ124-144
Lipofectamine 2000 + plasmid
10 µm
C
Untreated
Brefeldin A
MG132
ApoL9-V5Δ111-123
D
ApoL9-V5Δ124-144
E
ApoL9-V5
LAMP1
Merge
Inset
B16F10L9Δ111-123
B16F10L9Δ124-144
Bafilomycin A1

Fig.6: Properties of the region(s) of ApoL9 essential for PE-binding

A. Protein-lipid overlay assay for screening PE-binding in MBP-ApoL9 deletion mutants. 1 mg of dipalmitoyl-PE was spotted in quadruplicate on nitrocellulose membrane. Red asterisks indicate mutants that failed to bind PE. **B.** Immunostaining for ApoL9-V5 after lipofection of the insert-less vector *pBApo-EF1α pur* into cell lines stably expressing wild type ApoL9 or ApoL9 transmembrane deletion mutants for 4 h. Note the characteristic DOPE-induced aggregation only in WT. **C, D.** Subcellular distribution pattern of ApoL9Δ111-123 and ApoL9Δ124-144 electroporated into B16F10 cells and treated with 10 mg/mL brefeldin A for 18 h, or 10 mM MG132 for 6 h. Note the difference in pattern after MG132 treatment. **E.** Indirect immunofluorescence for ApoL9-V5 and LAMP1 in B16F10$^{L9\Delta111\text{-}123}$ and B16F10$^{L9\Delta124\text{-}144}$ after treatment with 200 nM bafilomycin A1 for 16 h. Boxed insets are magnified for better viewing.

Figure 7

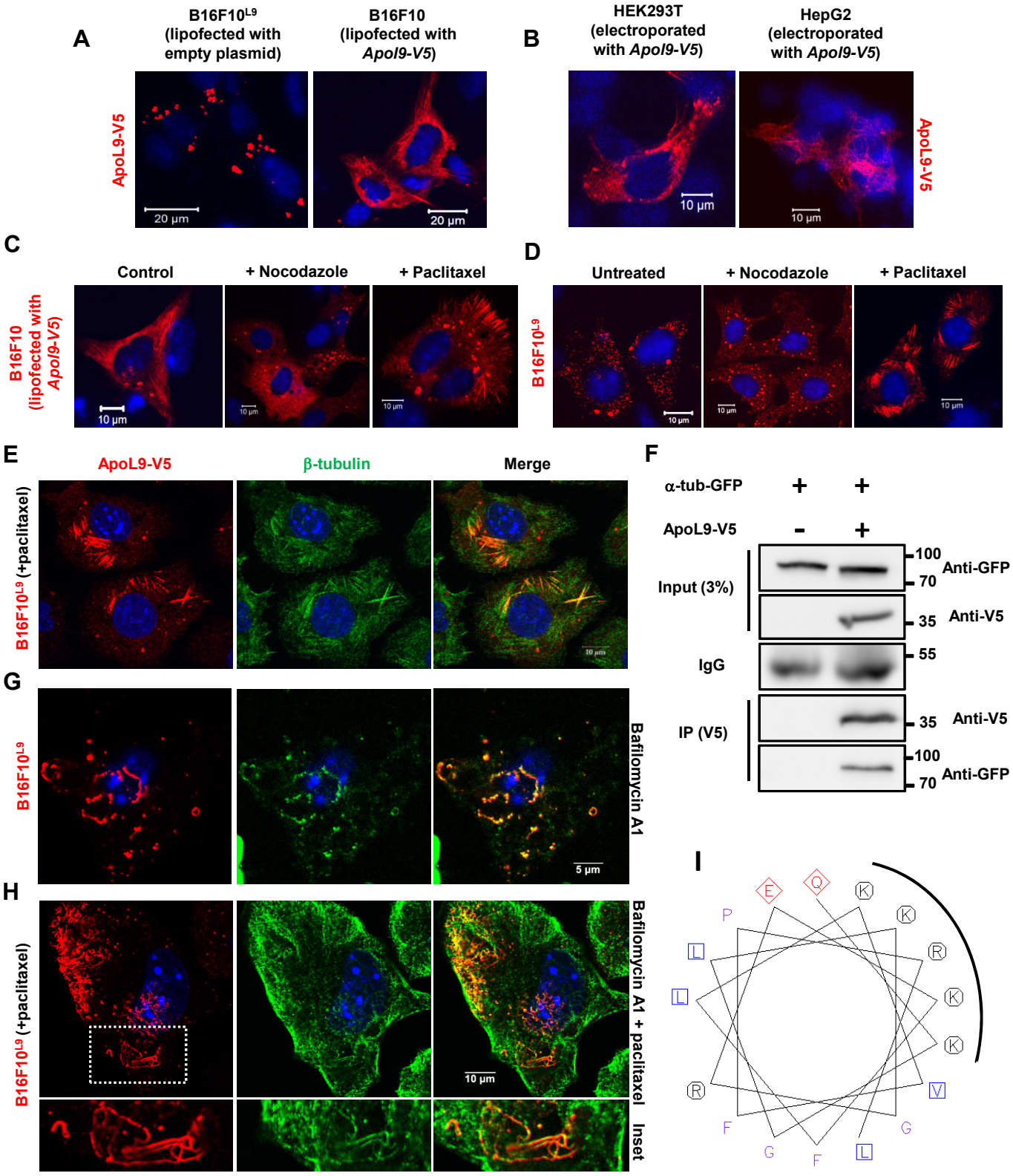
A
B16F10L9 (lipofected with empty plasmid)
B16F10 (lipofected with Apol9-V5)
ApoL9-V5
20 µm
20 µm
B
HEK293T (electroporated with Apol9-V5)
HepG2 (electroporated with Apol9-V5)
ApoL9-V5
10 µm
10 µm
C
Control
+ Nocodazole
+ Paclitaxel
B16F10 (lipofected with Apol9-V5)
10 µm
D
Untreated
+ Nocodazole
+ Paclitaxel
B16F10L9
E
ApoL9-V5
β-tubulin
Merge
B16F10L9 (+paclitaxel)
F
α-tub-GFP + +
ApoL9-V5 - +
Input (3%)
IgG
IP (V5)
100
70
Anti-GFP
35
Anti-V5
55
35
Anti-V5
100
70
Anti-GFP
G
B16F10L9
Bafilomycin A1
5 µm
H
B16F10L9 (+paclitaxel)
Bafilomycin A1 + paclitaxel
10 µm
Inset
I
E
Q
K
K
R
K
K
V
G
L
G
F
R
L
L
P

Fig.7: ApoL9 is a microtubule-associated protein

A. Difference in distribution pattern of ApoL9 when insert-less plasmid *pBApo-EF1α pur* is lipofected into B16F10^{L9} cells versus when *Apol9-V5* cloned in *pBApo-EF1α pur* is lipofected into B16F10 cells. **B.** The *Apol9-V5* construct was electroporated into HEK293T and HepG2 cells. Note the fibre-like structures in the cytoplasm. **C, D.** Effect of compounds that affect microtubule stability on ApoL9 distribution in (C) B16F10 cells lipofected with *Apol9-V5* and in (D) B16F10^{L9} cells. Paclitaxel was used at 10 mM for 4 h and nocodazole at 10 mg/mL for 3 h. **E.** Co-localization of ApoL9-V5 and β-tubulin in B16F10^{L9} cells treated with paclitaxel for 10 h. Anti-b-tubulin antibody was used. **F.** Co-immunoprecipitation of GFP-tagged alpha tubulin with ApoL9-V5 from lysates of HEK293T cells transfected with both constructs. Cells transfected with control vector and the alpha tubulin construct were used as a negative control. **G, H.** Immunoblotting for ApoL9-V5 and β-tubulin in B16F10^{L9} cells treated with bafilomycin (18h) only or with paclitaxel added for the last 8 h. Note the presence of tubulin in curved, thread-like structures. We found tubulin localization in these structures to be sporadic/weak and not seen in all cells. **I.** The region of the helix comprising amino acids 54-70 of mouse ApoL9a, viewed as a helical wheel at http://www.bioinformatics.nl/cgi-bin/emboss/pepwheel . Note the basic residues clustered on one side of the helix.

Figure 8

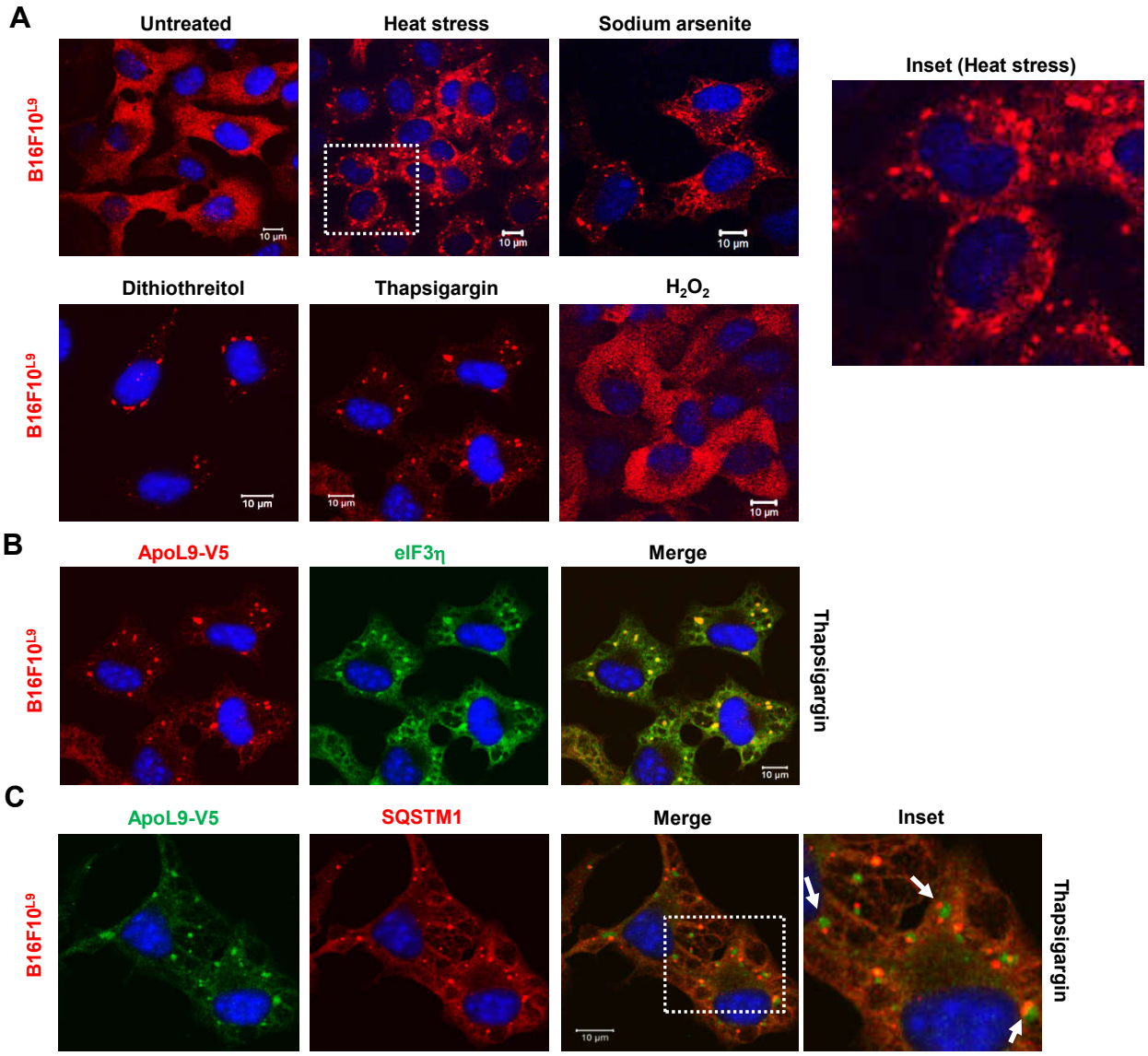

Fig.8: Localization of ApoL9 in stress granules

A. Distribution pattern of ApoL9-V5 in B16F10^{L9} cells after treatment with various stress-inducing agents as indicated. Boxed inset (heat stress) is magnified and shown. **B.** Indirect immunofluorescence for ApoL9-V5 and stress granule marker eIF3η in B16F10^{L9} cells treated with 500 nM thapsigargin for 1 h. Anti-eIF3η was used. **C.** Indirect immunofluorescence in thapsigargin-treated B16F10^{L9} cells to distinguish ALIS/sequestosomes (stained with anti-SQSTM1 antibody) from stress granules (stained with anti-V5 antibody). Note the proximity between both types of granules in the magnified inset.